Deep expression of the Indonesian Throughflow: Indonesian Intermediate Water in the South Equatorial Current

Lynne D. Talley and Janet Sprintall

Scripps Institution of Oceanography, University of California, San Diego, La Jolla, California, USA

Received 29 November 2004; revised 8 April 2005; accepted 7 June 2005; published 8 October 2005.

[1] The narrow westward flow of the South Equatorial Current (SEC), centered at 12°S and carrying freshened water from the Indonesian seas, is traced across the Indian Ocean using data from the World Ocean Circulation Experiment. The jet is remarkably zonal and quasi-barotropic, following the potential vorticity contours characteristic of the tropics, separating higher-oxygen and lower-nutrient waters of the subtropics from the oxygen-depleted waters of the tropics. The fresh surface waters are the usual Indonesian Throughflow Water reported previously. Less well studied is the intermediate-depth SEC carrying fresher water from the Banda Sea and Pacific, known as Indonesian Intermediate Water (IIW) or Banda Sea Intermediate Water. The high-silica signature of IIW is documented here, permitting us to (1) trace the spread of IIW from sill density at Leti Strait to higher density as it is diluted toward the west and (2) define an IIW core for transport estimates, of 3 to 7 Sv westward, using geostrophic and LADCP velocities. The high IIW silica is traced to the Banda Sea, arising from known diapycnal mixing of Pacific waters entering through Lifamatola Strait and local sources. New heat, freshwater, oxygen, and silica budgets within the Indonesian seas suggest at least 3 Sv of inflow through the relatively deep Lifamatola Strait, supplementing the observed 9 Sv through the shallower Makassar Strait. Both shallow and deep inflows and outflows, along with vigorous mixing and internal sources within the Indonesian seas, are required to capture the transformation of Pacific to Indonesian Throughflow waters.

Citation: Talley, L. D., and J. Sprintall (2005), Deep expression of the Indonesian Throughflow: Indonesian Intermediate Water in the South Equatorial Current, *J. Geophys. Res.*, *110*, C10009, doi:10.1029/2004JC002826.

1. Introduction

[2] In the global thermohaline circulations described by *Gordon* [1986], *Broecker* [1991], *Schmitz* [1995], and modeled by *Blanke et al.* [2001] and *Speich et al.* [2001], among others, the warm water portion of the overturn includes westward flow from the Pacific through the Indonesian passages where it is significantly transformed by mixing and internal sources. The product, Indonesian Throughflow (ITF) water, enters the Indian Ocean, flows westward in the South Equatorial Current (SEC), enters the Agulhas, and then moves onward to the Atlantic, joining the global circulation.

[3] Description of the throughflow waters crossing the Indian Ocean has mostly focused on the very low salinity upper ocean layer [e.g., *Gordon et al.*, 1997]. These warm and relatively fresh waters from the surface to the upper thermocline are referred to as Indonesian Throughflow Water (ITW) [*Fieux et al.*, 1994]. A deeper core to the throughflow has also long been recognized. Because the minimum sill depth between the Pacific and Indian is 1250 m, at Leti Strait at the eastern end of the Timor Trench [*Van Bennekom*, 1988] (Figure 1b), a signature of Pacific water to at least this depth should be expected in the Indian Ocean, and is indeed found. The Pacific-Indonesian origin of the intermediate depth salinity minimum at ~1000 dbar between 11° and 14°S in the tropical Indian Ocean was identified by *Rochford* [1961, 1966] and *Wyrtki* [1961], and is independent from the salinity minimum of the Indian Ocean's Antarctic Intermediate Water [*Talley and Baringer*, 1997]. *Rochford* [1961, 1966] called this salinity minimum Banda Sea Intermediate Water (BSIW). We follow *Emery and Meincke* [1986], *Van Aken et al.* [1988], *Fieux et al.* [1994, 1996a], *You* [1998b], and *Wijffels et al.* [2002], and refer to BSIW as Indonesian Intermediate Water (IIW) to reflect its Pacific and Indonesian origin. IIW also has a marked silica signature that persists far to the west along the SEC, as described in detail here. Other chemical tracers also reflect the Pacific origin of the IIW, including ^{3}He [*Jean-Baptiste et al.*, 1997; *Top et al.*, 1997].

[4] The ITF in Makassar Strait has a volume transport that at 9–10 Sv [*Gordon et al.*, 1999; *Vranes et al.*, 2002] is equivalent to midlatitude meridional Ekman transports. The deeper portion of the ITF, supplied through Lifamatola Strait, should be included in discussions of the total throughflow, yielding a larger total transport than is usually assumed, by at least 2–3 Sv [*Gordon et al.*, 2003]. The ITF is potentially an important element of heat transport in the Southern Hemisphere [*Macdonald*, 1993; *Robbins and*

0148-0227/05/2004JC002826$09.00

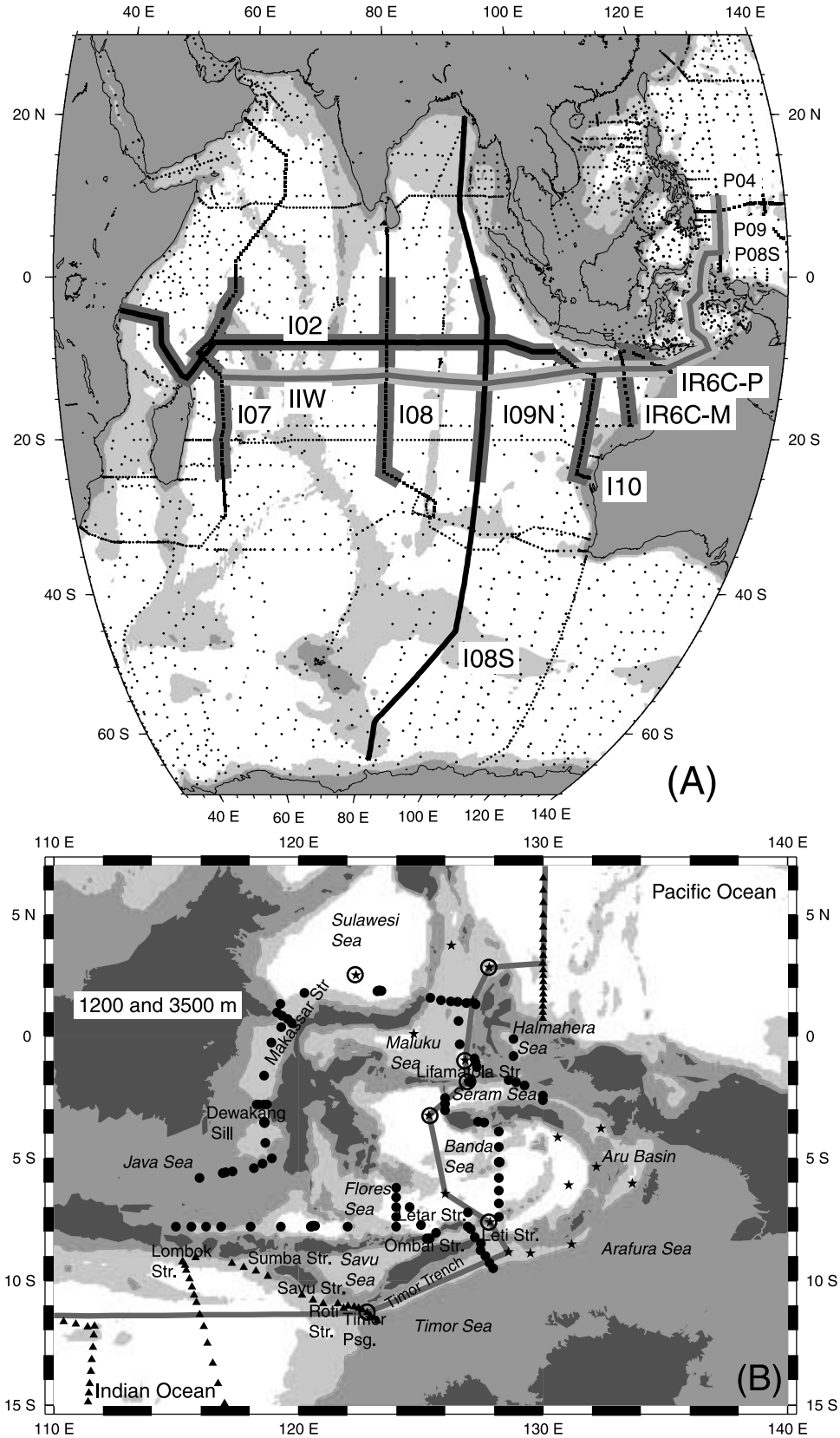
40 E
60 E
80 E
100 E
120 E
140 E
20 N
0
20 S
40 S
60 S
P04
P09
P08S
I02
IIW
I07
I08
I09N
IR6C-P
IR6C-M
I10
I08S
(A)
110 E
120 E
130 E
140 E
5 N
5 S
10 S
15 S
Pacific Ocean
Sulawesi Sea
1200 and 3500 m
Makassar Str
Maluku Sea
Halmahera Sea
Lifamatola Str.
Seram Sea
Dewakang Sill
Java Sea
Banda Sea
Aru Basin
Flores Sea
Letar Str.
Leti Str.
Ombai Str.
Arafura Sea
Lombok Str.
Sumba Str.
Savu Sea
Sayu Str.
Timor Trench
Roti Str.
Timor Psg.
Timor Sea
Indian Ocean
(B)

Figure 1

Table 1. Acronyms: Water Masses and Others

Acronym	Definition
AAIW	Antarctic Intermediate Water
BSIW	Banda Sea Intermediate Water
CDW	Circumpolar Deep Water
IDW	Indian Deep Water
IIW	Indonesian Intermediate Water
ITF	Indonesian Throughflow
ITW	Indonesian Throughflow Water
NIIW	North Indian Intermediate Water
SEISAMW	Southeast Indian Subantarctic Mode Water
ADCP	Acoustic Doppler Current Profiling
CTD	Conductivity-temperature-pressure
LADCP	Lowered ADCP
SEC	South Equatorial Current
WOCE	World Ocean Circulation Experiment

Toole, 1997], but its recently observed average temperature of 15°C in Makassar Strait [*Vranes et al.*, 2002] was lower than hypothesized, suggesting only a minor role [*Talley*, 2003]. Including the colder Lifamatola component in the *Talley* [2003] calculation would only further reduce the ITF impact on heat transport. In its influence on Pacific and Indian Ocean salinity, however, the ITF loop likely has a greater role than for heat (L. D. Talley et al., manuscript in preparation, 2005). Since the salinity of the Pacific waters entering the Indonesian Passages is fresher than the inflow from the Southern Ocean to the Pacific, the ITF represents a net transport of freshwater out of the Pacific into the Indian Ocean, where evaporation increase its salinity. Taking the Indian and Pacific together, the ITF loop transports freshwater northward out of the Southern Ocean since the northward transport into the Pacific is fresher than the southward transport in the Agulhas.

[5] The total ITF is thus composed of the ITW of the upper layer and the deeper IIW. The purpose of our paper is to provide a comprehensive, modern view of the IIW, which was last approached at the largest scale by *Rochford* [1966]. Data from WOCE and collected since WOCE within the Indonesian seas clearly update the older view. Our focus is a comprehensive treatment of IIW: its tracers, distribution, transport, and relation to potential vorticity within the Indian Ocean, and its source in the Pacific as modified by mixing and boundary fluxes within the Indonesian seas. Section 2 contains background, and section 3 contains the data sets. The lateral and vertical extent of IIW is identified through its vertical salinity minimum and meridional dissolved silica maximum (section 4). The volume transport of this deeper part of the throughflow is estimated (section 6), and its relationship to the large-scale potential vorticity field is explored (section 5). We find that the throughflow jet, from the sea surface down through this intermediate-depth portion, is remarkably zonal, extending along a strong front in the tropical Indian (South Equatorial Current), in a region where potential vorticity is almost exactly zonal [*McCarthy and Talley*, 1999].

[6] In section 7, we show the alteration of the Pacific properties within the Indonesian region and compute net flux convergences. The contorted pathway includes numerous sills and basins (Figure 1). For the researcher concerned with the large-scale impact of the throughflow, the minimum description must include both a shallow and a deep inflow, and a minimum of four outflow straits, major diapycnal mixing [e.g., *Van Bennekom*, 1988; *Gordon et al.*, 2003], and reasonable external sources (air-sea fluxes, etc.) within the region.

[7] Monsoons and interannual variability (ENSO and Indian dipole mode) affect upper and even deep ocean circulation in the tropical Indian Ocean, with maximum westward flow out of the Indonesian seas into the Indian Ocean during the southeast monsoon in August and September [e.g., *Meyers et al.*, 1995; *Meyers*, 1996; *Fieux et al.*, 1996b; *Schott and McCreary*, 2001]. Because we are concerned with a gross characterization of water mass properties, which persist regardless of the monsoon, and because extensive time series of hydrographic sections do not exist, we only briefly discuss monsoonal influence in conjunction with transport estimates in section 6.

[8] Acronyms are listed in Table 1. Potential densities are referenced to 1000 dbar throughout. Conversion of key densities to neutral density γ^n [*Jackett and McDougall*, 1997] and to potential density σ_θ referenced to 0 dbar is given in Table 2, using 100 stations from the WOCE section I9 at 95°E north of 30°S.

2. Background

2.1. Indonesian Throughflow Water in the Indian Ocean

[9] In the Indian Ocean, the surface waters originating from the Indonesian seas (ITW) are easily identified by their low salinity in the South Equatorial Current (SEC), which flows nearly due westward across the Indian Ocean [e.g., *Rochford*, 1966; *Gordon et al.*, 1997; *Talley and Baringer*, 1997]. ITW becomes saltier as it moves westward and spreads meridionally in the Indian Ocean, because of lateral mixing [*Gordon et al.*, 1997]. At 80°E, *Talley and Baringer* [1997] found that low-salinity Indonesian water (both ITW and IIW) is identifiable down to intermediate depths. They also showed that the SEC dominates all other dynamical features on the long transect from Sri Lanka to southern Australia. *You* [1998b] showed the presence of IIW in the SEC down through at least 1100 m depth.

[10] In their high-resolution diagnostic model of the Indonesian seas, *Miyama et al.* [1995] found a vertical distribution of ITF transport that agrees with observations

Figure 1. (a) Hydrographic station data from the World Ocean Circulation Experiment (WOCE) hydrographic programme (WHP; http://whpo.ucsd.edu/) and from A. J. Mantyla and J. L. Reid [*Mantyla and Reid*, 1995; *Reid*, 2003]. For the WOCE data, thick shaded lines indicate sections in Figure 6; thin lines indicate sections in Figure 2. Other WOCE and historical data are indicated by small dots. The 500 and 3500 m isobaths (etopo5) are shaded. (b) Indonesian passages region. Data are shown as follows: WOCE (triangles), 1994 Arlindo (circles), and 1976 Indopac (stars). Circled stations are used in Figure 16. The shaded line is a section constructed from WOCE and Indopac data. The 1200 m and 3500 m isobaths (etopo5) are shaded.

Table 2. Equivalent Potential Density and Neutral Surfaces for 100 Stations Along 95°E North of 30°S

Potential Density σ_1 Relative to 1000 dbar	Neutral Density γ^n	Potential Density σ_θ Relative to 0 dbar	Pressure, dbar
31.5 σ_1	27.116 ± 0.009	27.02 ± 0.02	577 ± 85
31.7 σ_1	27.297 ± 0.007	27.19 ± 0.03	729 ± 60
31.9 σ_1	27.413 ± 0.003	27.36 ± 0.02	931 ± 37
31.96 σ_1	27.525 ± 0.002	27.41 ± 0.02	1010 ± 34
32.1 σ_1	27.656 ± 0.004	27.52 ± 0.02	1259 ± 24
32.2 σ_1	27.758 ± 0.007	27.602 ± 0.02	1463 ± 31

at the exit to the Indian Ocean: ~10 Sv in the upper 400 m, a local minimum below this, and a local maximum transport of ~5Sv occurring at ~1250 m [*Fieux et al.*, 1994; *Molcard et al.*, 1996]. This deeper part of the model transport is fed by a westward deep current (1000–1500 m) in the equatorial Pacific, like that observed by *Luyten and Swallow* [1976], *Leetmaa and Spain* [1981] and *Firing* [1989]. The Pacific water enters via the eastern route through Lifamatola Passage (Figure 1b) and mixes with waters from the North Pacific. The model trajectories of particles at 1250 m as they enter the Indian Ocean flow zonally across the Indian Ocean.

[11] *Wijffels et al.* [2002] found that the local minimum in westward flow at ~ 470 m depth [*Fieux et al.*, 1994; *Molcard et al.*, 1996] coincides with a vertical salinity maximum in the SEC. The salinity maximum is due to admixture of salinity maximum waters from the subtropical gyre to the south and Arabian Sea Water to the north (see Figure 6 below). The ITW and IIW would lose their low salinity more slowly than the salinity maximum layer during westward advection across the Indian Ocean because the adjacent waters on their isopycnals (surface layer and AAIW) are considerably fresher than the other Indian Ocean waters. We concentrate here on the IIW when discussing water properties, but include the ITW and salinity maximum layer when computing transports.

[12] IIW is marked by high silica as well as low salinity. *Reid* [2003] shows a tongue of high silica extending westward at 32.0σ_1 (~1050 dbar) across the Indian Ocean from the Indonesian seas. A similar high-silica tongue is positioned north of the equator, with its high silica apparently acquired in the eastern Bay of Bengal. The two westward extending tongues are separated by an eastward extending tongue of low silica at the equator. This equatorial symmetry extends to great depth (sections 4 and 5).

[13] Other chemical tracers also mark the IIW. *Jean-Baptiste et al.* [1997] documented an elevated ^{3}He signal at 1200–1250 m in the eastern Indian Ocean, on the World Ocean Circulation Experiment (WOCE) IR6C (JADE 89) section between Australia and Bali (Figure 1a). *Top et al.* [1997] also found elevated ^{3}He signals at ~1100–1200 m along the Bali-Timor transect, highest at stations capturing the outflow from Savu Strait and Timor Passage. The ^{3}He plume is possibly evidence of intermediate-depth flow from the Pacific to the Indian Ocean since the Pacific is enriched in ^{3}He compared with the Indian. Although additional deep ^{3}He sources are found locally in the Sulawesi Sea and Makassar Strait, *Top et al.* [1997] hypothesized that they do not influence the Indian Ocean because of the shallow Dewakang Sill. Another mantle source at 2500 m depth in the Flores Sea may participate in a deep overturning cell with the Banda Sea at these depths [*Top et al.*, 1997].

2.2. Indonesian Seas

[14] Flow from the Pacific to the Indian through the Indonesian seas is complex, with every sill providing a mixing site to form the low-salinity water characteristic of the ITF [e.g., *Gordon et al.*, 2003]. The major routes are (1) in the west [*Gordon and Fine*, 1996; *Hautala et al.*, 1996] through the Sulawesi Sea (blocked below 1350 m) into Makassar Strait and Dewakang sill (650 m deep) and (2) in the east through the Maluku Sea (blocked below 2340 m) into Lifamatola Strait (1940 m sill), or directly over the Halmahera Sea (blocked below 700 m) into the internal Seram and Banda seas (Figure 1b). From the Banda Sea, the ITF exits into the southeast Indian Ocean via Timor Passage (1250 m eastern sill depth at Leti Strait, and 1890 m at the western end), or through Ombai Strait (sill depth 3250 m) and thence through Sumba Strait (900 m) and Savu Strait (1150 m).

[15] Upper thermocline waters in the Indonesian seas are primarily from the North Pacific subtropical waters and North Pacific Intermediate Water flowing southward in the Mindanao Current [*Lukas et al.*, 1991; *Gordon*, 1995; *Fine et al.*, 1994; *Gordon and Fine*, 1996]. The Dewakang sill permits only the upper thermocline waters to enter the Flores and Banda seas, or to exit directly into the Indian Ocean via the shallow (350 m) Lombok Strait. Smaller contributions of North Pacific surface water enter via the Maluku Sea [*Gordon and Fine*, 1996]. Upper waters of South Pacific origin enter via the Halmahera Sea [*Hautala et al.*, 1996]. Lower thermocline and deeper water masses (AAIW and Circumpolar Deep Water or CDW) enter the Indonesian seas via the deeper eastern route through Lifamatola Strait. They originate in the South Pacific from the New Guinea Coastal Undercurrent. These are saltier than the North Pacific upper waters (see figures in section 7).

[16] As mentioned above, IIW is also called "Banda Sea Intermediate Water" after the deep internal basin (Figure 1b) where most transformation of the deeper Pacific waters occurs. As the Pacific water masses enter, they mix diapycnally, with a region-averaged rate greater than 10^{-3} m^2/s [*Van Aken et al.*, 1991; *Gordon et al.*, 2003], to form the distinctive Indonesian water profile of relatively isohaline water from the thermocline to near the bottom [*Ffield and Gordon*, 1992; *Hautala et al.*, 1996; *Waworuntu et al.*, 2000; *Gordon et al.*, 2003]. The proximity of major property changes to sills [*Gordon et al.*, 2003] suggests that most diapycnal mixing occurs there rather than at interior locations where mixing is relatively weak (<10^{-4} m^2/s) [*Alford et al.*, 1999]. Intense vertical mixing of Pacific water has been documented at Lifamatola Passage [*Van Aken et al.*, 1988; *Van Bennekom*, 1988] and over the Halmahera sill [*Van Aken et al.*, 1988; *Ilahude and Gordon*, 1996]; of Indian Ocean water over the sills between the eastern basins from Timor Trench, the Aru Basin, and up into the Seram Sea [*Van Riehl*, 1943; *Postma and Mook*, 1988; *Van Bennekom*, 1988; *Fieux et al.*, 1994]; and of mixed Banda Sea Intermediate Water between the Flores and western Banda Sea basins [*Gordon et al.*, 1994]. At least some of this diapycnal mixing is due to tides [*Ffield*

and Gordon, 1996]. Density driven flow of deep water over the sills may also drive deep circulation patterns that keep the internal basins well ventilated. The deeper waters upwell and vertically mix with the overlying less dense water up to depths of 500–600 m [*Van Bennekom et al.*, 1988; *Van Aken et al.*, 1988; *Hautala et al.*, 1996; *Gordon et al.*, 2003]. Horizontally, there are gradients in salinity across the Banda Sea, reflecting water masses from the North Pacific (maximum in the western Banda Sea) and South Pacific (maximum in the eastern Banda Sea) [*Ilahude and Gordon*, 1996; *Hautala et al.*, 1996; *Waworuntu et al.*, 2000].

3. Data Sets and Methods

[17] The data for this study are World Ocean Circulation Experiment (WOCE) Hydrographic Programme stations in the Indian and Pacific oceans (Figure 1a), and historical hydrographic data from the 2001 World Ocean Database (WOD2001). The WOCE data (http://whpo.ucsd.edu/) are a uniformly high quality data set, with station spacing of 55 km or closer along sections, and sampling to the ocean bottom. At each station there is a CTD profile with temperature, salinity and pressure at 2 dbar intervals, and bottle sampling at up to 36 depths. Water samples were analyzed for salinity, oxygen, nutrients and other tracer chemicals (not used here). All have underway acoustic Doppler current profiling (ADCP). Many stations included lowered ADCP (LADCP). The historical hydrographic data from *Mantyla and Reid* [1995] and *Reid* [2003] extend to the ocean bottom and include dissolved silica.

[18] Data for the Indonesian seas include a 1976 R/V *T. Washington* cruise (''Indopac'') with silica and oxygen [*Broecker et al.*, 1986], and the Arlindo Mixing project, with 103 hydrographic CTD stations during the southeast monsoon in August-September 1993, and 105 (mostly repeat) hydrographic stations during the northwest monsoon of January-February 1994 [*Gordon*, 1995; *Gordon and Fine*, 1996; *Ilahude and Gordon*, 1996; *Gordon et al.*, 2003]. Other WOD2001 data supplemented these specific cruises.

[19] The 2-dbar CTD data were smoothed using a 10-dbar half-width Gaussian filter and then linearly interpolated to the desired potential density, referenced to 1000 dbar (σ_1). Bottle data were interpolated vertically to 10-dbar intervals using an Akima cubic spline and then linearly interpolated to isopycnals. Isopycnic potential vorticity $(f/\rho)(\partial\rho/\partial z)$ was calculated from both bottle and CTD data. *McCarthy and Talley* [1999] show the correspondence of potential vorticity interpolated from bottle data with that calculated from CTD data smoothed with a Gaussian of 50 dbar vertical half width. *Roemmich*'s [1983] objective mapping method was used for vertical sections. For isopycnal maps, the station data were mapped to a uniform grid using the blockmedian and surface algorithms in the GMT mapping package [*Smith and Wessel*, 1990], and then contoured using the GMT grdcontour algorithm [*Wessel and Smith*, 1998].

[20] Zonal transports for the meridional WOCE sections were calculated from the 2 dbar CTD data. Uncertainty in the synoptic transports was estimated by variously referencing them to 0 cm/s at the bottom, to the shipboard and lowered ADCP velocities, and to absolute reference velocities for each station pair from *Reid* [2003] (J. Reid, personal communication, 2003).

4. Indonesian Intermediate Water Properties (Salinity and Dissolved Silica)

[21] The intermediate-depth portion of the Pacific waters that enter the Indian Ocean through the Indonesian passages can be traced in those water properties that differ greatly between the Indian and Pacific. Salinity (section 4.1) and dissolved silica (section 4.2) are particularly useful and abundant observations. The SEC structure is considered in the context of the potential vorticity distribution in section 5. The South Equatorial Current (SEC) advects the IIW westward; its structure and transport are considered in section 6. Eddying or recirculation on the north side of the SEC [*Hacker et al.*, 1998] spreads the IIW as far north as the zonal WOCE section at 8°S.

[22] Three chokepoints constrain the flow of deeper Pacific waters through the Indonesian seas, and are marked on the salinity and dissolved silica sections that cover the Indian to the Pacific through the Indonesian seas (Figures 3 and 11 below). Leti Strait, at 1250 m, is the saddle depth for the ITF, with a sill density of 32.08 σ_1. Lifamatola Strait, at 1940 m, regulates the flow of deep Pacific water into the interior Indonesian seas. The potential density at this depth on the WOCE P8S stations is $32.33\sigma_1$. Therefore waters at this density and above can enter and be mixed in the Banda Sea. However, as shown in section 7 below, the maximum density found within the internal Indonesian seas does not exceed $32.25\sigma_1$, presumably because of strong mixing at Lifamatola Strait and net heating within the seas. Downstream of Leti Strait, Timor Passage, which is 1890 m deep with a sill density of 32.34 σ_1 (from adjacent IR6C stations), limits the backflow of Indian Ocean water into the Timor Sea.

4.1. Salinity in the Tropical Indian Ocean: The Indonesian Intermediate Water

[23] The Indonesian Throughflow waters are apparent in the open Indian Ocean on a representative meridional section at 95°E (Figure 2) as the low-salinity surface water (ITW) and the deeper salinity minimum (IIW) between about 8°S and 17°S. The other major salinity features at 95°E are as follows. The high salinity of the Indian Deep Water in the north originates from evaporation in the Red Sea and Arabian Sea. The thin layer of fresh surface water at the northern end of this 95°E section is due to river runoff into the Bay of Bengal [e.g., *Shetye et al.*, 1991; *Zhang and Talley*, 1998]. High-salinity surface waters between 20°S and 43°S, with an equatorward extending salinity maximum (Subtropical Underwater), are the typical evaporative waters of the subtropical gyre. The subsurface salinity minimum of the subtropical gyre is the Antarctic Intermediate Water (AAIW), whose origin is around Drake Passage [*McCartney*, 1977; *Talley*, 1996]. The source of high salinity in the Circumpolar Deep Water (CDW) (in the Antarctic Circumpolar Current south of 43°S) is North Atlantic Deep Water. At the bottom is the fresher Lower Circumpolar Deep Water (Antarctic Bottom Water), formed around the margins of Antarctica.

[24] As a function of potential density (Figure 2b), the low-salinity IIW centered at about $31.95\sigma_1$ in the narrow

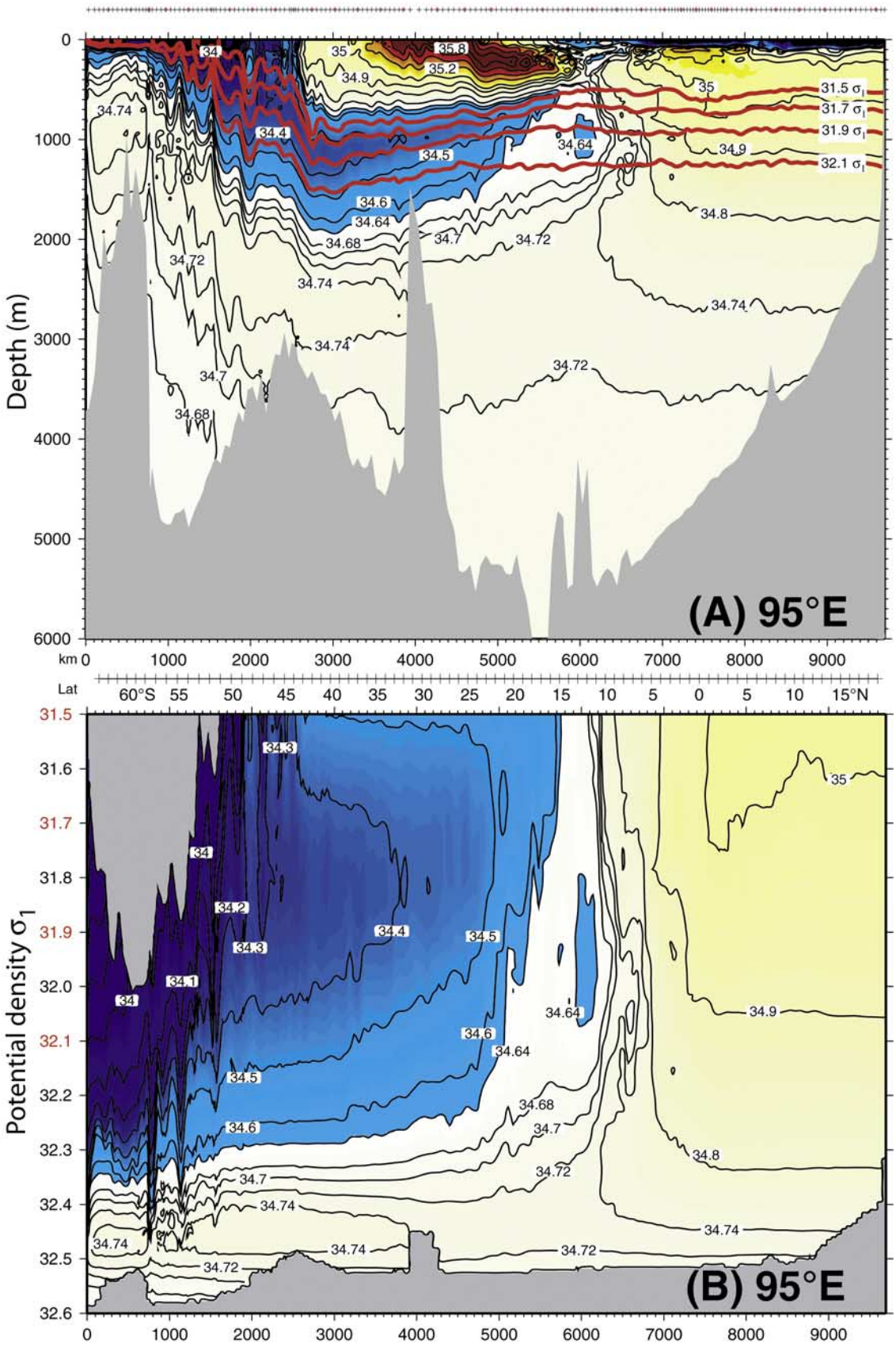

Figure 2. Full depth salinity sections along 95°E (I9N and I8S) as a function of (a) depth and (b) potential density σ_1. A selected set of potential density σ_1 levels is shown in red in each panel. Station positions are shown in Figure 1.

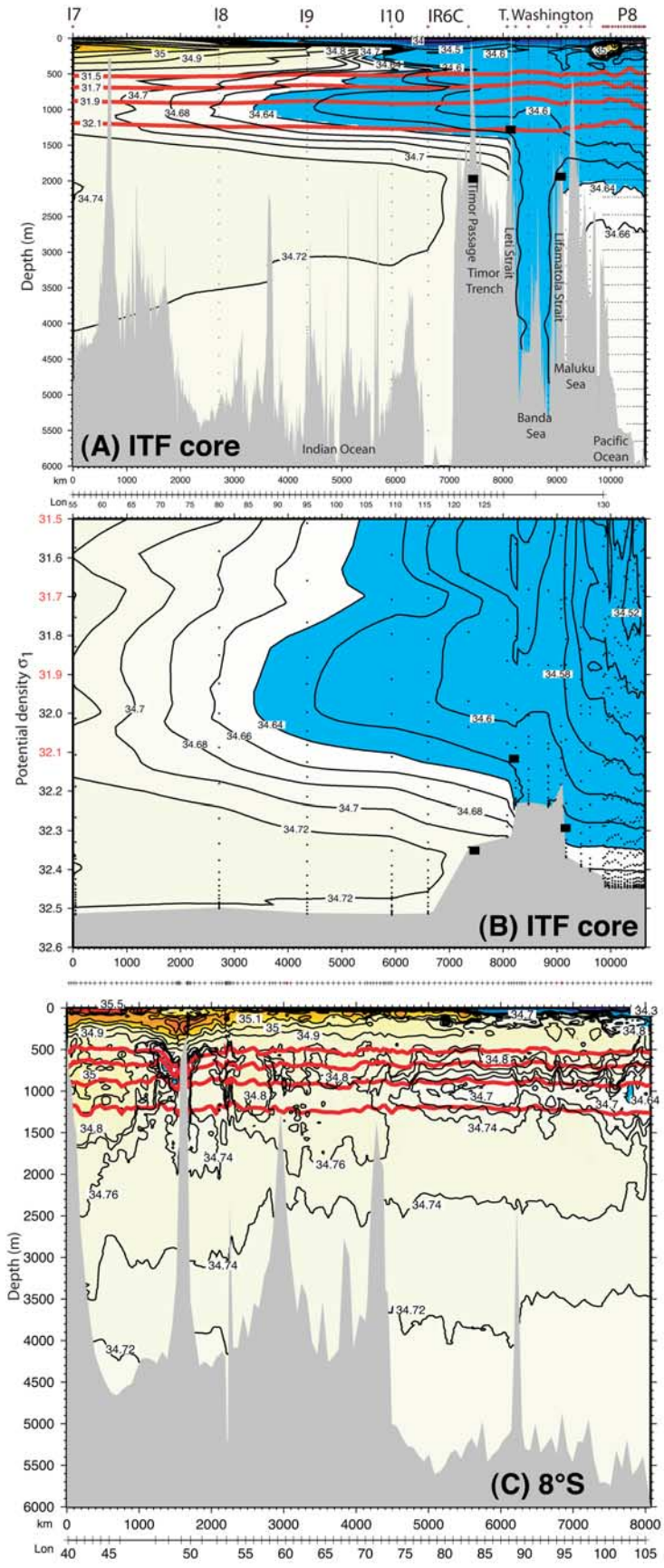
I7
I8
I9
I10
IR6C
T. Washington
P8
Depth (m)
(A) ITF core
Indian Ocean
Timor Passage
Timor Trench
Leti Strait
Lifamatola Strait
Maluku Sea
Banda Sea
Pacific Ocean
km
Lon
Potential density σ1
(B) ITF core
Depth (m)
(C) 8°S
km
Lon

Figure 3

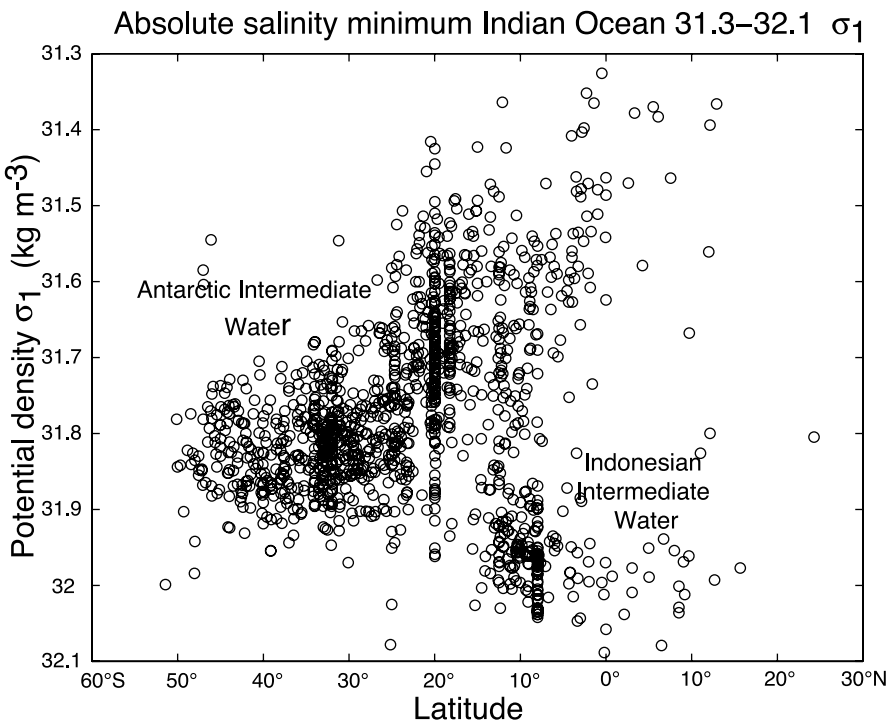

Figure 4. Absolute salinity minimum at each historical hydrographic station (Figure 1a) in the density range 31.3–32.1σ_1. The cluster of salinity minima at 31.7–31.9σ_1 and south of 20°S is Antarctic Intermediate Water (AAIW). The cluster of minima at 31.85–32.0σ_1 and north of 18°S is Indonesian Intermediate Water (IIW) (also known as Banda Sea Intermediate Water).

South Equatorial Current contrasts with the adjacent saltier waters. (When Figure 2b is extended upward to lower densities, the fresh ITW is obvious at densities less than 31.30σ_1.) The IIW sits in the lower part of an "hourglass" shape in the salinity contours with the ITW in the upper part.

[25] The fresh ITW and IIW separate the northern (equatorial) and southern waters with a nearly vertical boundary on the north side of the salinity minima. Below the IIW, the same vertical boundary extends down to at least 2500 m, separating the higher-salinity Indian Deep Water (IDW) to the north from slightly fresher waters at midlatitude. The nearly uniform salinities along isopycnals in the well-defined water mass regimes to the north and south are noteworthy, for instance, in the subducted high-salinity layer of the south Indian Ocean's subtropical gyre, and in the deep waters in both the north and south. A second, laterally separated, slightly denser (32.05σ_1) salinity minimum occurs at 8°S, north of the SEC, slicing into the higher-salinity equatorial waters. This northern minimum also appears on the other meridional sections described below. It is likely within an eastward circulation, fed and perhaps driven by lateral eddying from the SEC (section 6), as a deeper expression of the recirculation cell between the upper SEC and equatorial currents [*Gordon et al.*, 1997].

[26] The westward penetration of the low-salinity IIW at about 1000 dbar across the Indian Ocean is traced clearly with stations within the IIW (SEC) from each of the meridional WOCE sections (Figures 3a and 2b). The salinity core spreads nearly isopycnally (Figure 3b), at densities between 31.8 and 32.0σ_1. A high gradient in salinity at the bottom of the core is also evident, associated with the sill depth of the deepest exit passages from the Indonesian seas (Sumba, Savu, Roti and Timor). The penetration of low salinity to the bottom in the Banda Sea is a dramatic feature (section 7). However, when viewed isopycnally, the drama disappears, and the salinity is seen to be a continuation of low salinity at similar densities in the neighboring Pacific.

[27] The zonal WOCE I2 section at 8°S (Figure 3c) is within the weak secondary salinity minimum north of the IIW core (Figure 2a). Even though the salinity minimum is saltier than along the IIW core (Figure 3a), it is fresher at the eastern boundary and more saline to the west, just like the IIW core. This suggests that its source is either local eddying/diffusion from the IIW or westward advection from an eastern boundary source of somewhat higher salinity

Figure 3. Full depth salinity sections along the core of the Indonesian Intermediate Water (South Equatorial Current), through the Banda Sea, and northward at 130°E in the Pacific (P8) as a function of (a) depth and (b) potential density σ_1; (c) 8°S (I2) as a function of depth. Station positions are shown in Figure 1. Bathymetry in Figure 3a is from *Smith and Sandwell* [1997]. In Figures 3a and 3b, the short black bars indicate the maximum sill depth and density. A selected set of potential density σ_1 levels is shown in red in each panel.

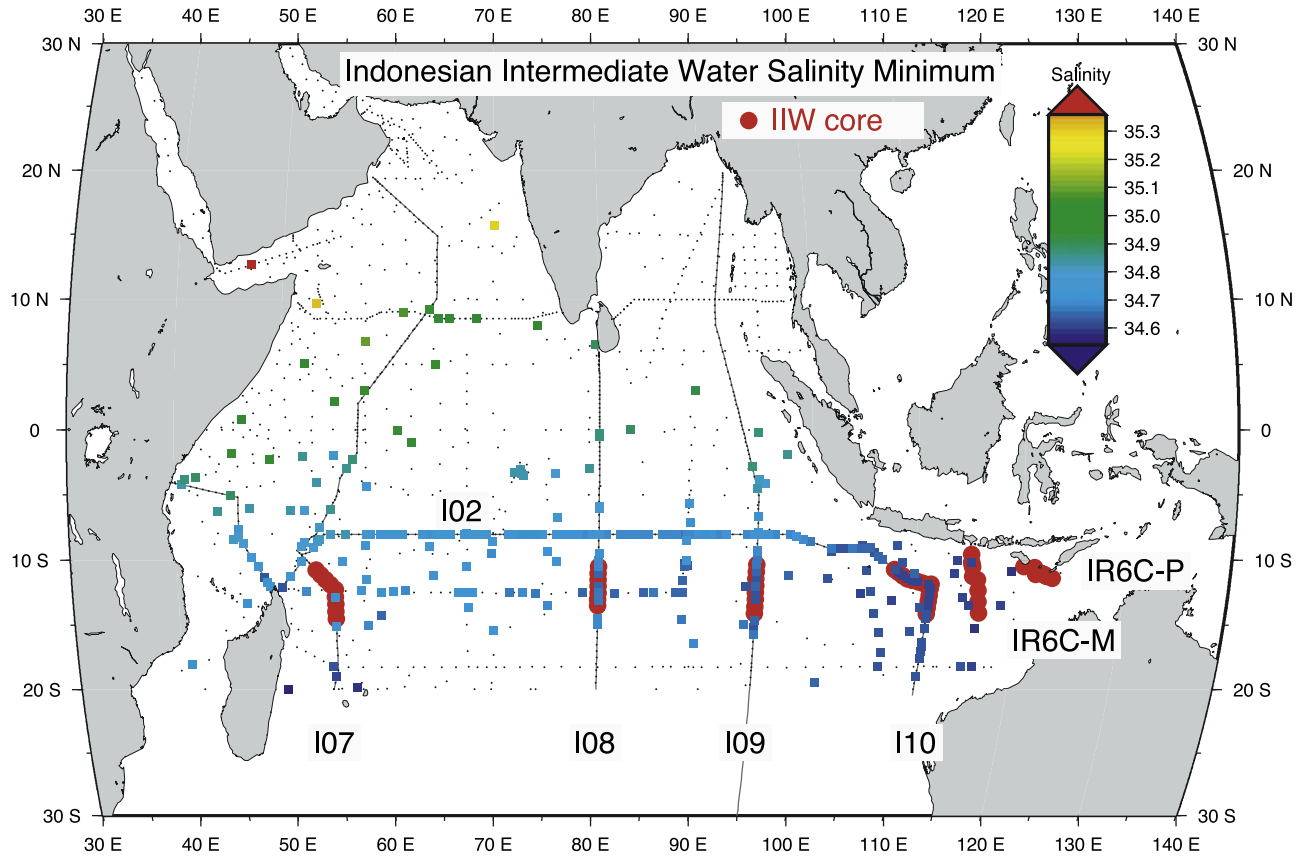

Figure 5. Stations with Indonesian Intermediate Water (IIW) salinity minimum (large squares), as defined in section 3; colors indicate salinity (psu). Red underlying circles indicate WHP stations at the IIW core, as defined by the silica/salinity relation (Figure 11 below); stations at IR6C and I7 do not have the salinity minimum.

than the IIW. Velocity sections examined in section 6 indicate eastward flow in this secondary minimum, hence supporting the eddying hypothesis. This secondary salinity minimum breaks up west of 73°E. Low-salinity IIW reappears in the west at about 50°E where the I2 section dips southward to Madagascar, entering the central IIW core. The deeper (1500 m) salinity minimum at the same location near Madagascar is the northward penetration of AAIW. The surface signature of ITW is also apparent. High salinity on the zonal section comes from the Arabian Sea surface waters in the west, and Indian Deep Water centered at 800 dbar, which originates as high-salinity water in the Red Sea.

[28] How do we differentiate the IIW (the main salinity minimum centered around 10°S) from the AAIW of the subtropical gyre? The absolute salinity minima in the AAIW and IIW density range ($31.3-32.1\sigma_1$) from all Indian Ocean hydrographic stations show clear separation between the AAIW and IIW (Figure 4). The IIW is north of 18°S and is somewhat denser than AAIW. AAIW is mainly located south of 20°S, centered at 31.8 σ_1, shifting upward to lower densities within the tropical latitudes of the IIW. This upward extension of a salinity minimum that is eroding (becoming more saline) is typical of the largest-scale interleaving of such water masses (for instance the Labrador Sea Water and Mediterranean Water), and may result from large-scale double diffusive processes. *You* [1998a] suggested that salt-fingering double diffusion might occur at these densities in the western tropical Indian Ocean, as the cool, fresher AAIW encounters the overlying warm, salty Indian Central Waters. The separate identity of IIW is especially supported through salinity/silica relations (section 4.2).

[29] To map the IIW (Figure 5), all salinity minima north of 20°S in the density range $31.83-32.1\sigma_1$ were identified. This density range was selected to avoid including the eroding AAIW. The IIW is centered at 14°S, and is best defined in a band between about 8°S and 18°S. Thus the zonal WOCE I2 section at 8°S (Figure 3c), which has the secondary salinity minimum associated with IIW, is not representative of the main westward extending IIW core, as discussed in reference to Figures 2 and 3. Each mid-ocean meridional section does have a band of eastward flow north of the SEC (section 6), suggesting a recirculation of the main IIW jet [*Gordon et al.*, 1997; *Hacker et al.*, 1998].

[30] Individual meridional sections of salinity and potential density (Figure 6) and potential temperature/salinity within the IIW core (Figure 7) show the low-salinity IIW and its westward salinity increase. The nominal location of the IIW on each WOCE section and its core density, salinity, and silica are listed in Table 3. Where the ITF exits the Indonesian seas in Timor Passage (Figure 6f), the entire water column is relatively fresh, except for a remnant of saline Arabian Sea Water

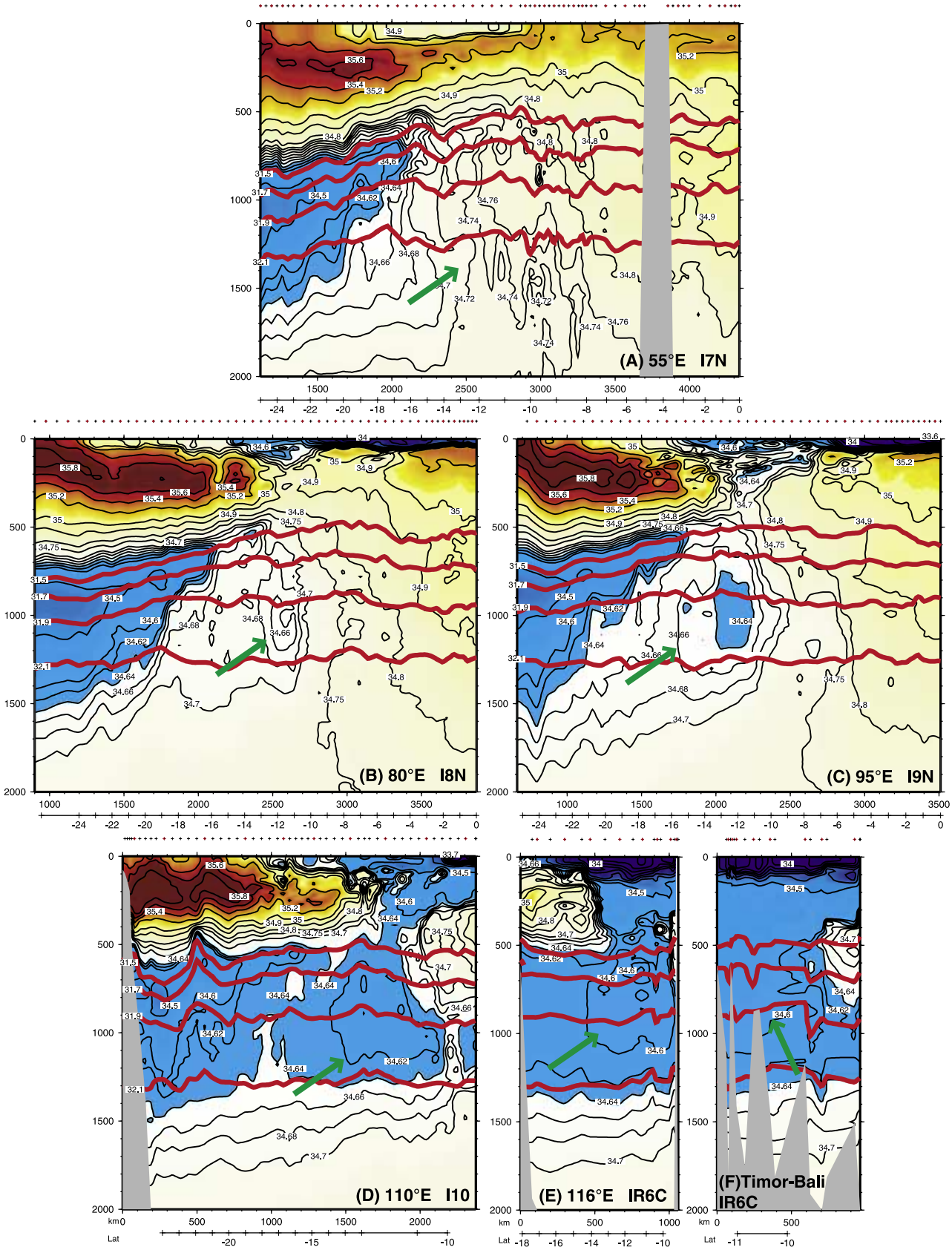
(A) 55°E I7N
(B) 80°E I8N
(C) 95°E I9N
(D) 110°E I10
(E) 116°E IR6C
(F)Timor-Bali
IR6C
km
Lat

Figure 6

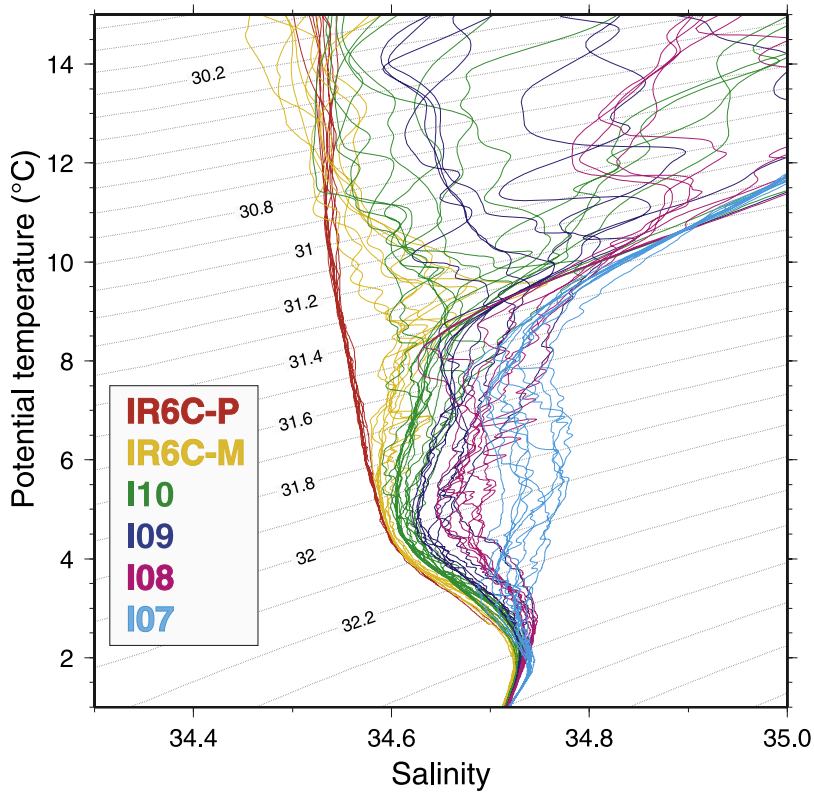

Figure 7. Potential temperature versus salinity for stations within the core of the South Equatorial Current (Indonesian Intermediate Water). Contours of potential density relative to 1000 dbar (σ_1) are superimposed. Station locations are shown in red in Figure 5.

to the north. The IIW salinity minimum is already formed, and centered at 10–11°S, 350–1100 m (34.6 psu contour), at the southern end of this short section, directly west of Timor Strait.

[31] Just a few degrees of longitude west of Timor Strait, on the IR6C (JADE 89) section between Bali and Australia (Figure 6e), the low-salinity (<34.6 psu) IIW is near the northern boundary (Bali coast), between 10°S and 14°S and 500–1100 m. The full thickness of the ITF-influenced layer is apparent here, from the surface to the bottom of this intermediate water. At the next section to the west, 110°E (Figure 6d), the IIW salinity is slightly higher (core defined by 34.62 psu, with the full increase apparent in Figure 7). High-salinity subtropical and equatorial waters encroach more between the IIW and the surface ITW. AAIW is apparent in the south, against Australia. These points were noted by *Wijffels et al.* [2002].

[32] Continuing farther west, the 95°E and 80°E sections show the isolated IIW, with higher core salinities (Figure 7), and the overall salinity minimum defined well by 34.68–34.69 psu (Figures 6b and 6c). The high-salinity subtropical surface water and IDW are more saline than at 110°E. At 80°E (Figure 6b), the IIW core splits into two or more pieces, with an intrusion into the higher-salinity equatorial waters up to 6–7°S. The low-salinity AAIW erodes upward to a lower density as it approaches the IIW core in the SEC jet. A salinity front separates the AAIW from the SEC salinity features, just as the northern edge of the SEC is marked by a salinity front at the IIW level.

[33] In the far west, at 55°E (Figure 6a), the IIW core is broken and difficult to interpret. The low-salinity surface layer ITW is still apparent between 11° and 18°S [*Gordon et al.*, 1997]. Salinity minima at around 600 m most likely are a northward extension of the AAIW. Salinity minima centered at 1500 m could be remnants of IIW, but could also be due to mixing of the high-salinity North Indian Intermediate Water [*Rochford*, 1961, 1966] and IIW, forming a "new" water mass in the western equatorial Indian Ocean that then flows back eastward at depth against the deep SEC and northern edge of the AAIW [*Rochford*, 1961, 1966; *Wijffels et al.*, 2002].

[34] There has been some examination of the entry of IIW into the Agulhas system in the western Indian Ocean [*Warren*, 1981; *You*, 1998b]. Warren indicates the difficulty of separating IIW and AAIW within the lower-salinity waters at 18°S east of Madagascar. You's mixing analysis shows the difficulty of locating the IIW after it reaches the western Indian Ocean: the nearly exactly

Figure 6. Tropical upper ocean meridional sections of salinity (color and black contours) and potential density 31.5, 31.7, 31.9, and 32.1 σ_1 (red contours): (a) 55°E (I7), (b) 80°E (I8), (c) 95°E (I9), (d) 110°E (I10), (e) 116°E (IR6C "M"), and (f) Timor-Bali Passage (IR6C "P"). Locations are the thick shaded lines in Figure 1. Green arrows indicate the salinity minimum, used in Figures 10, 13, and 14.

Table 3. Indonesian Intermediate Water Properties at the Core Salinity Minimum and Silica Maximum[a]

Section (WOCE Identifier)	Station Numbers[b]	IIW Latitude Range[b] (Recirculation Salinity Minimum)	Depth Range[b]	Density, σ_1	Salinity, psu	Latitude	Depth of Minimum Salinity in the IIW	Maximum Density of Isopycnal Silica Maximum
Savu Strait, Timor Passage (IR6C-P)	26–37	9.5°–11°S	undefined (no salinity maximum) to 1150 m	31.66	34.571	11°S	589 ± 30 m	not applicable
116°E (IR6C-M)	8–16	9.5°–14°S	500–1100 m	31.70	34.583	10°30′S	689 + 18 m	$32.36\sigma_1$, 1934 ± 51
110°E (I10)	1056–1068	10°–14.5°S	500–1200 m	31.86	34.598	11°50′S	851 ± 36 m	$32.36\sigma_1$, 1931 ± 42
95°E (I9)	180–187	10°–16°S (6°–9°S)	500–1400 m	31.98	34.622	13°S	1024 ± 25 m	$32.34\sigma_1$, 1851 ± 29
80°E (I8)	327–333	10.5°–17°S (8.5°–10°S)	550–1400 m	31.98	34.646	12°S	1038 ± 18 m	$32.36\sigma_1$, 1918 ± 22
55°E (I7)	716–724	11°–14°S (8.5°–12°S)	1250–1700 m	32.24	34.709	12°49′S	1541 ± 44 m	$32.36\sigma_1$, 1910 ± 39

[a]Mean latitude 11.9°S ± 1.0°.
[b]Ranges are based on anomalous salinity/silica relation (Figure 12).

zonal axis of high IIW concentration simply dissipates, rather than moving directly either northward or southward. He concludes that it splits about equally into northward and southward flow at the Madagascar/African coasts. *Reid* [2003] does not show the deeper parts of the SEC reaching Madagascar.

[35] In summary, the IIW becomes saltier, slightly denser, deeper and more eroded toward the west. The latitude of the core, that is, the SEC, is nearly constant. A secondary salinity minimum just north of the IIW is apparently fed from the main SEC IIW. Salinity on the isopycnal $31.96\sigma_1$ (Figures 8 and 9) also shows the IIW's westward salinification, as well as the weak meridional salinity minimum along isopycnals (except at 55°E) that was used to define the core of the IIW.

4.2. Dissolved Silica in the Tropical Indian Ocean

[36] The IIW portion of the SEC is marked by higher silica on isopycnals compared with the surrounding Indian Ocean waters [*Wyrtki*, 1973; *You and Tomczak*, 1993; *Talley and Baringer*, 1997; *Reid*, 2003]. The high-silica IIW jet appears clearly at $31.96\sigma_1$ (Figure 9b), which lies within the IIW salinity minimum. The map is similar to *Reid*'s [2003] map at $32.0\sigma_1$, except that here the addition of Pacific Ocean data and sparse Indonesian passage data shows the Pacific origin of the high silica, with transformation in the Indonesian seas [*Broecker et al.*, 1986; *Van Bennekom*, 1988] (section 7 below).

[37] The high-silica IIW is flanked by lower-silica CDW to the south and by an equatorial tongue of low-silica Red Sea water (high salinity in Figures 2, 8, and 9). A separate westward extending high-silica tongue is centered at 5°–10°N. We find no connection of this Northern Hemisphere feature with the IIW – the eastern boundary South Java Current flows southward from the equator, and indeed, silica is low at the equator. Thus its high silica originates in the Bay of Bengal, perhaps from local sediments enriched by the major river outflows, hydrothermal sources, or upwelled high-silica deeper waters [*Edmond et al.*, 1979; *Gordon et al.*, 2002] (Figures 10 and 11).

[38] The equatorial symmetry of the high-silica tongues on the isopycnal map (Figure 9b) is striking, suggesting eastward flow in the broad equatorial band flanked by westward flows in both hemispheres, as mapped by *Reid* [2003] extending down to at least 3000 m. A similar set of symmetric tongues, suggesting reversing flows, is apparent in the Pacific and Atlantic [*Talley and Johnson*, 1994]. *You*'s [1998b] water mass distributions indicate the same equatorial symmetry, with high-silica IIW in the SEC, lower-silica AAIW along the equator, and a higher-silica pool in the Bay of Bengal. He ascribed the latter to IIW since he used no other high-silica intermediate water masses in the mixing analysis.

[39] The IIW's silica enhancement is also apparent on vertical sections (represented by 95°E in Figure 10) although the signal is subtle because of the overall increase of silica with depth [*Mantyla and Reid*, 1983, 1995]. The South Equatorial Current (ITW) is marked in the upper ocean at 13°S by a lateral (isopycnal) maximum of higher silica separating very low silica in the subtropical gyre and somewhat higher silica in the equatorial Indian Ocean. Below this narrow maximum, middepth silica contours bow upward marking the IIW. Both the ITW and IIW silica enhancements are clearest as a function of potential density (Figure 10b; also Figures 8 and 9). The SEC front extends much deeper than this middepth IIW tongue: high silica in the deep water from the Bay of Bengal is abruptly truncated at the SEC latitude, with a similar truncation in high salinity from the Red Sea Water (Figure 2) at middepth.

[40] We differentiated between IIW and AAIW in section 4.1 and Figure 4 on the basis of salinity alone. When silica is also considered, the separation is even clearer (Figure 12). In each panel, all stations and samples from the indicated WOCE section are included, including silica from the Pacific WOCE sections just outside the entrance to the Indonesian seas (Figure 12f). The Northern Hemisphere silica values form a clean envelope on the high-salinity side of each diagram, except in the far western Indian Ocean at 55°E (Figure 12a). The low-salinity side of the envelope is set by the southernmost stations, characterized by AAIW. Stations in the Southern Hemisphere tropics with a mixture of waters fall between the AAIW and Northern Hemisphere curves. Stations at the core of the IIW, which was defined from the salinity minimum (Figures 5 and 7), are clear in

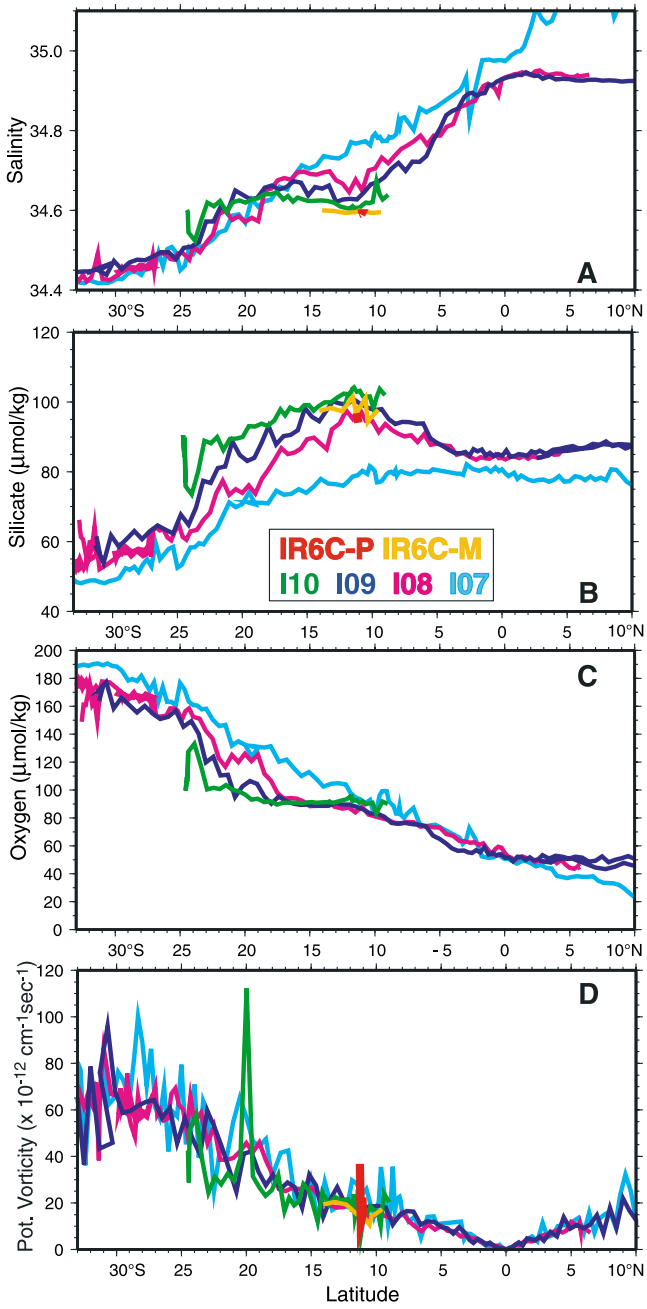

Figure 8. (a) Salinity, (b) dissolved silica (µmol/kg), (c) oxygen (µmol/kg), and (d) isopycnic potential vorticity ($\times 10^{-12}$ cm^{-1} s^{-1}) at 31.96 σ_1 for the meridional WOCE sections. This surface is equivalent to the neutral surface $\gamma^n = 27.52$.

each panel (except perhaps at 55°E) because of their low salinity at high silica (i.e., the elbow rising above the AAIW and Southern Hemisphere curves at 95–115 µmol/kg silica). The silica/salinity relation in the IIW core is tight and has the same shape all the way upstream through the Indonesian passages and into the Pacific (Figures 12e, 12f, and 13d).

[41] At the westernmost section at 55°E (Figure 12a), the obvious IIW core is missing from the silica/salinity relation. On the other hand, at 55°E, the stations between the southernmost and Northern Hemisphere stations have coalesced to the silica/salinity relation of the ITW/IIW stations at 95°E and 80°E. Thus either mixing between the northern and Southern Hemisphere source waters or the presence of ITW/IIW (or both) accounts for the silica/salinity relation in the South Equatorial Current at 55°E.

[42] The maximum density of the meridional silica maximum on each section (Table 3) is used to define the bottom of the IIW for transports (section 6 and Table 4). The maximum is at about 32.25σ_1 at 95°E (Figure 10). The bottom of the IIW as it emerges into the Indian Ocean is approximately the maximum density at Timor Passage. (Indian Ocean water within Timor Passage affects the Banda Sea properties exiting Leti Strait, and modifies the IIW.) As discussed in section 7, this is denser than at the chokepoint sill depth through the Indonesian seas (at Leti Strait) and thus indicates mixing of ITF water downward as it passes westward through Timor Trench.

5. Relation of the SEC to the Potential Vorticity Distribution

[43] Why is the SEC, from the sea surface to 2000 dbar, almost exactly zonal? A primary clue is in the distribution of isopycnic potential vorticity (Figure 9c) [*McCarthy and Talley*, 1999]. Following *McCarthy and Talley* [1999], we plot the stretching and planetary vorticity components, ignoring relative vorticity,

$$Q = -f/\rho(\partial\rho/\partial z) \quad (1)$$

in which the vertical gradient is computed using the local vertical stability. In the tropics, Q is dominated by the planetary vorticity gradient, β. The southern limit of the zonal tropical potential vorticity regime can be identified as a higher meridional gradient, slanting from about 19°S in the west to 23°S in the east. This boundary is matched in the silica distribution (Figure 9b). Because of the nearly exact zonality of Q in the tropics, flow must also be nearly exactly zonal in the absence of external forcing. The SEC at 31.96σ_1 (Figures 8d and 9c) is well within this tropical potential vorticity regime.

[44] The SEC, based on salinity and silica (Figures 2, 6, and 10), is vertical and centered at 12°S. The IIW salinity minimum is shown in the vertical section of Q at 95°E (Figure 14), and lies in a "shoulder" of the tropical potential vorticity. (By "shoulder" we mean Q contours with a combination of gentle slope and an adjacent nearly vertical plunge, such as the contour 20×10^{-14} cm^{-1} s^{-1} at 10° to 15°S.) The higher gradient of potential vorticity south of the IIW, centered at about 20°S on this section, is especially evident when Q is contoured as a function of potential density (Figure 14b). At depth, salinity at 95°E (Figure 2) suggested a penetration of the SEC to at least 2500 dbar (32.45σ_1), and silica (Figure 10) to at least 4000 dbar. The transition in salinity below the IIW to the high-salinity Indian Deep Water corresponds to the transition from one Q layer with a "shoulder" to a separate deep layer with a similar feature located at 20° to 25°S.

[45] At shallower depths, the subtropical Q structure extends closer to the equator and is dominated by the low values of the Southeast Indian Subantarctic Mode Water

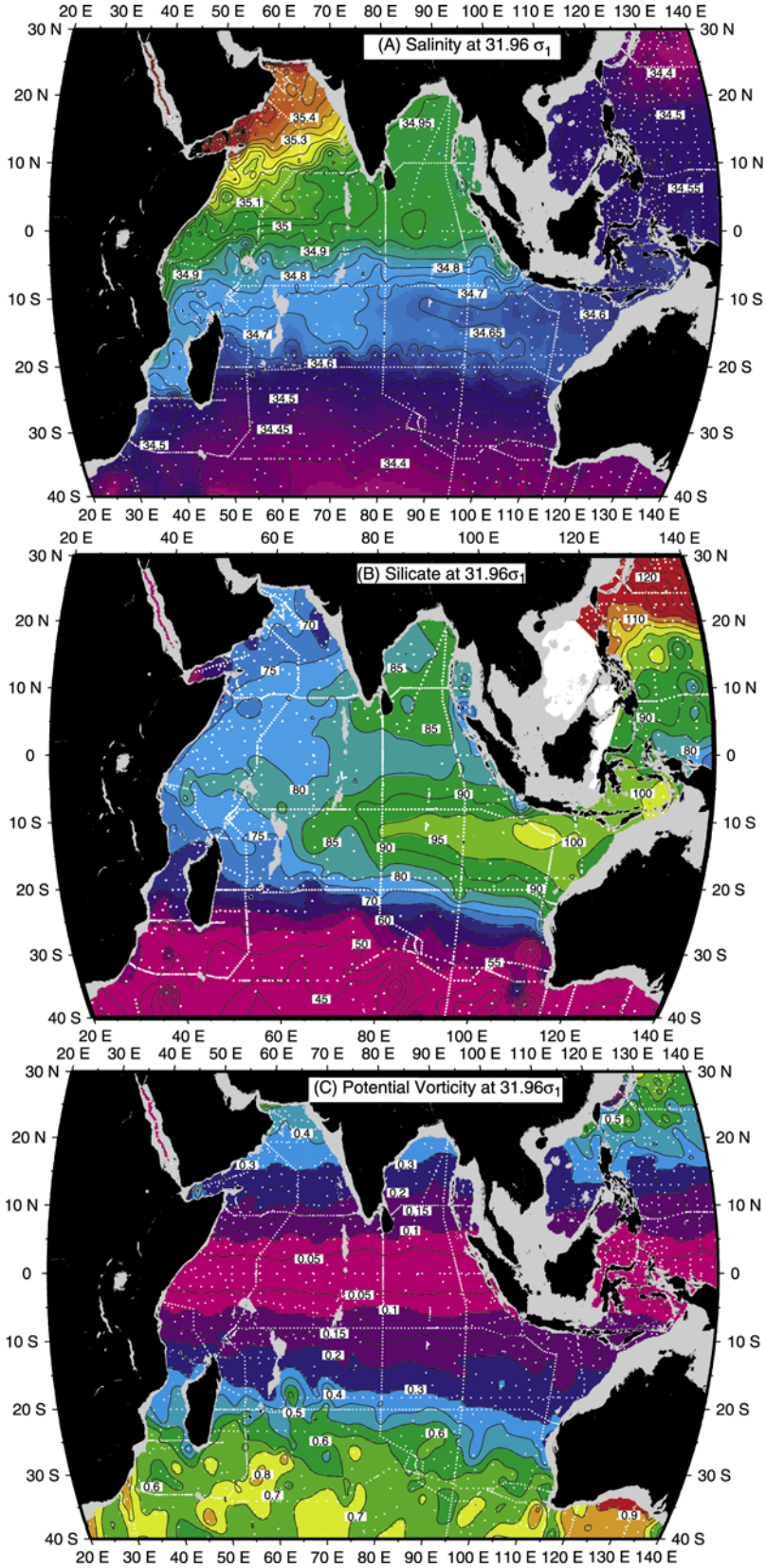

Figure 9. (a) Salinity, (b) dissolved silica (μmol/kg), and (c) absolute value of isopycnic potential vorticity ($\times 10^{-14}$ cm^{-1} s^{-1}) at 31.96 σ_1, including available stations in the Indonesian archipelago, Indian and Pacific WOCE sections, and historical data from the Pacific and Indian oceans [*Reid*, 1997, 2003]. This surface is equivalent to the neutral surface $\gamma^n = 27.52$.

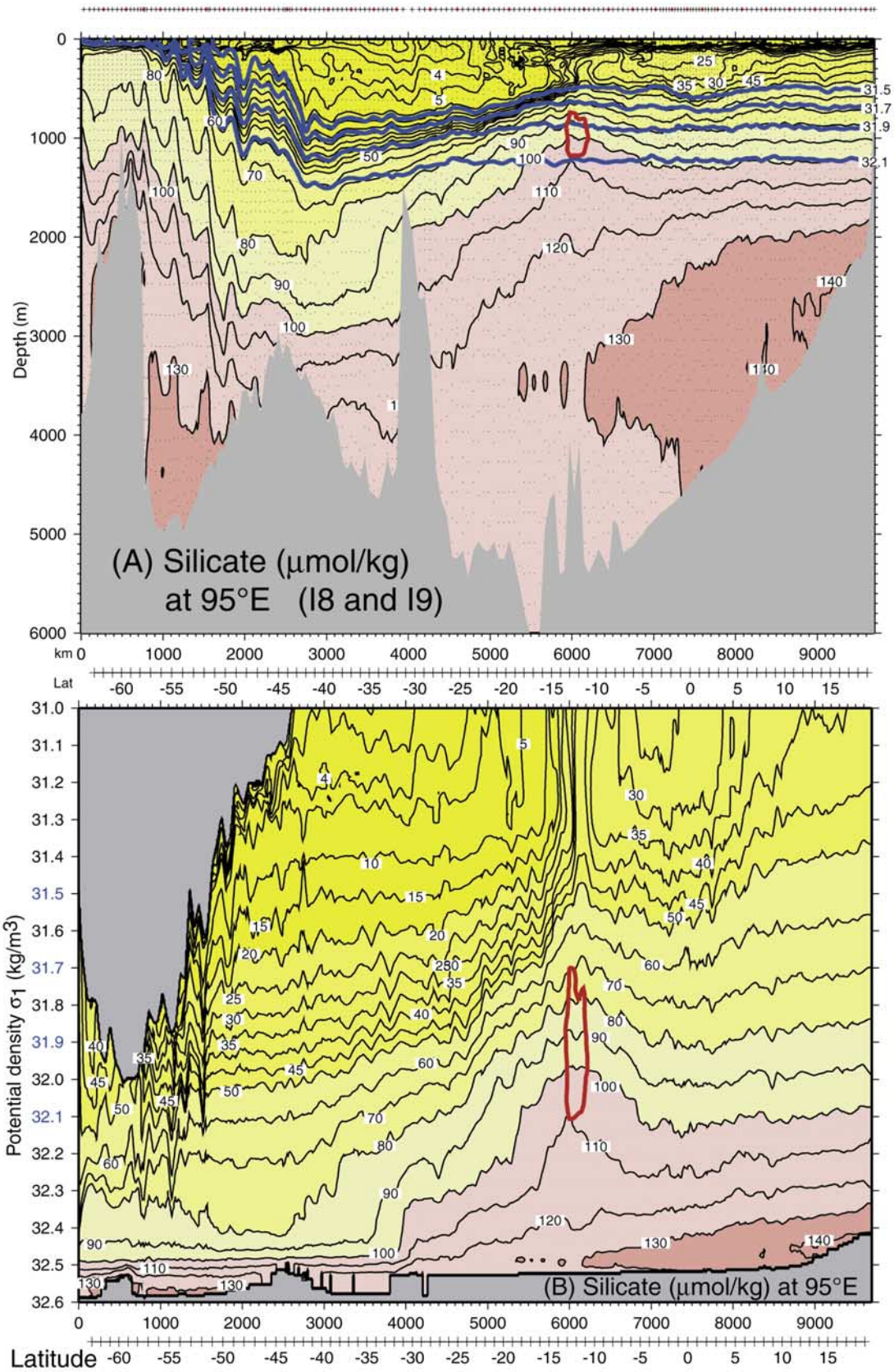

Figure 10. Dissolved silica (μmol/kg) for the WHP section at 95°E (I9N and I8S) as a function of (a) depth and (b) potential density σ_1. Blue curves in Figure 10a are potential density σ_1 contours. Station positions are shown in Figure 1a. The red curve in both panels is the IIW salinity minimum (S = 34.64 from Figures 2 and 3).

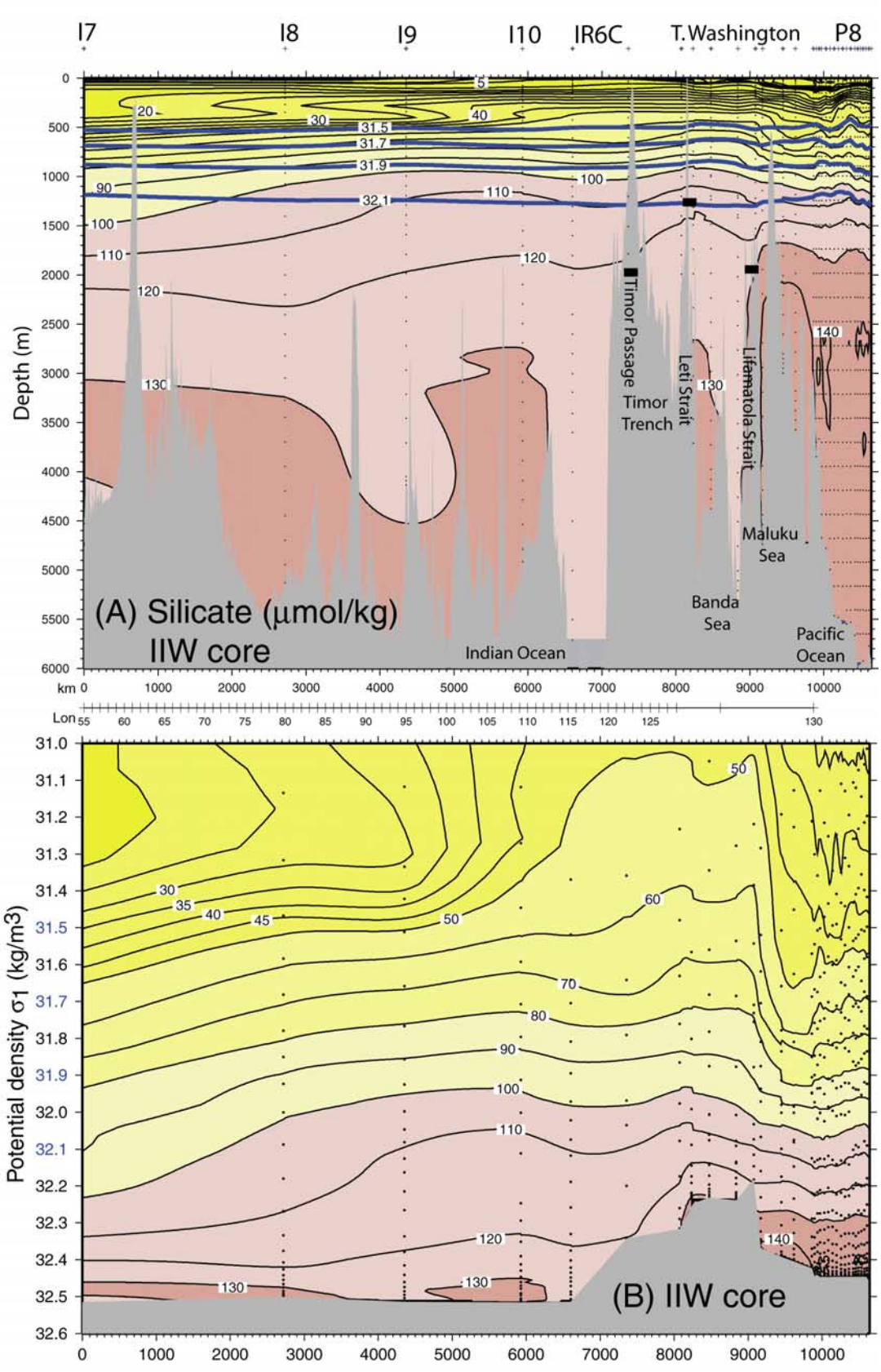

Figure 11. Dissolved silica (μmol/kg) for section along the core of the Indonesian Intermediate Water (South Equatorial Current) (approximately 14°S), through the Banda Sea, and Pacific WHP section P8S, as a function of (a) depth and (b) potential density σ_1. Station positions are shown in Figure 1a.

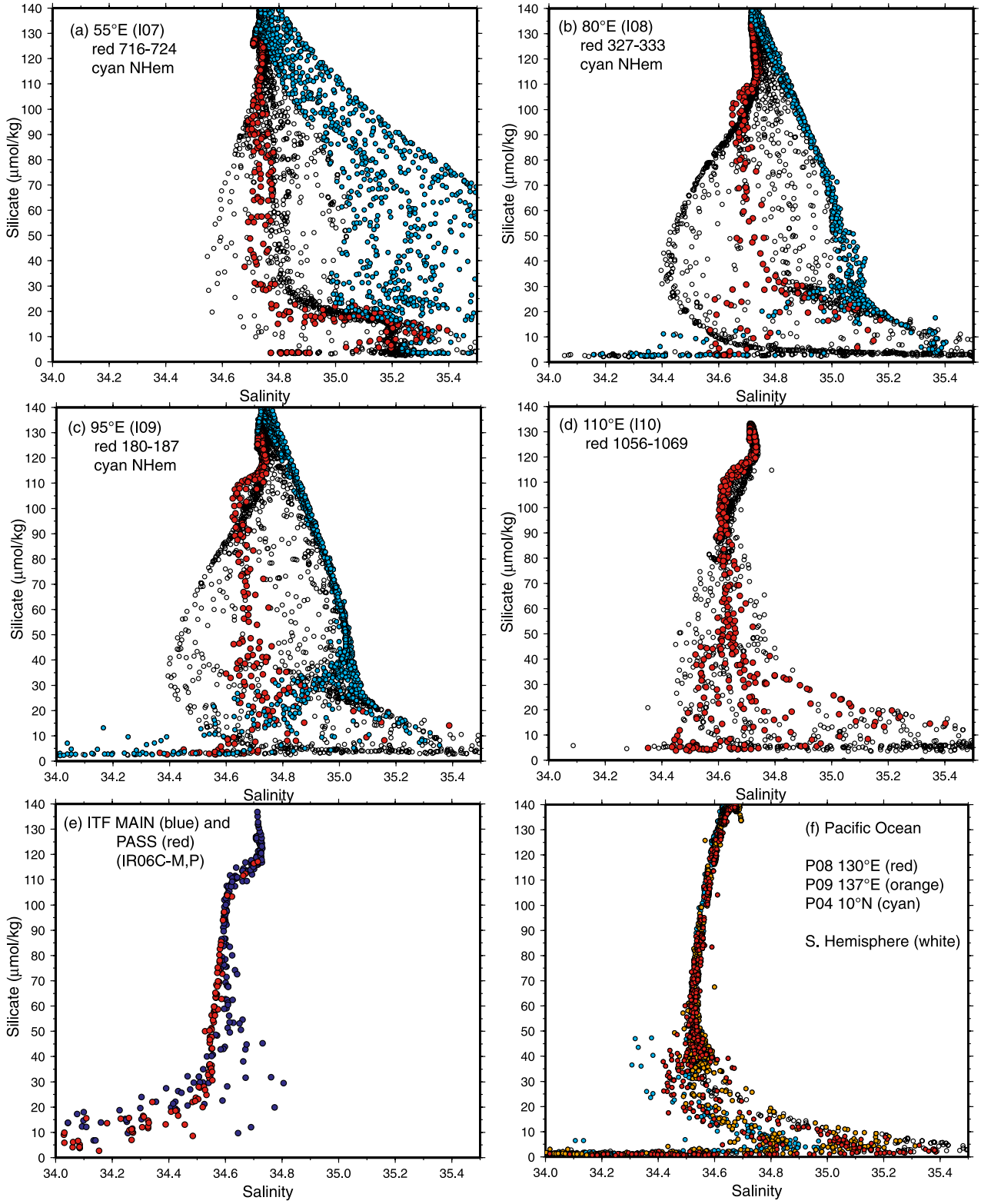

Figure 12. Dissolved silica (µmol/kg) as a function of salinity at (a) 55°E (I7), (b) 80°E (I8), (c) 95°E (I9), (d) 110°E (I10), (e) Bali-Timor Passage (IR6C) (red) and 116°E (IR6C) (blue), and (f) Pacific entrance (P08, P09, P04). In Figures 12a–12d, red circles (and also blue circles in Figure 12e) are stations in the South Equatorial Current (red circles in Figure 5); white circles (open circles) are all samples south of equator; and blue circles are samples north of equator. Station locations are shown in Figure 1a.

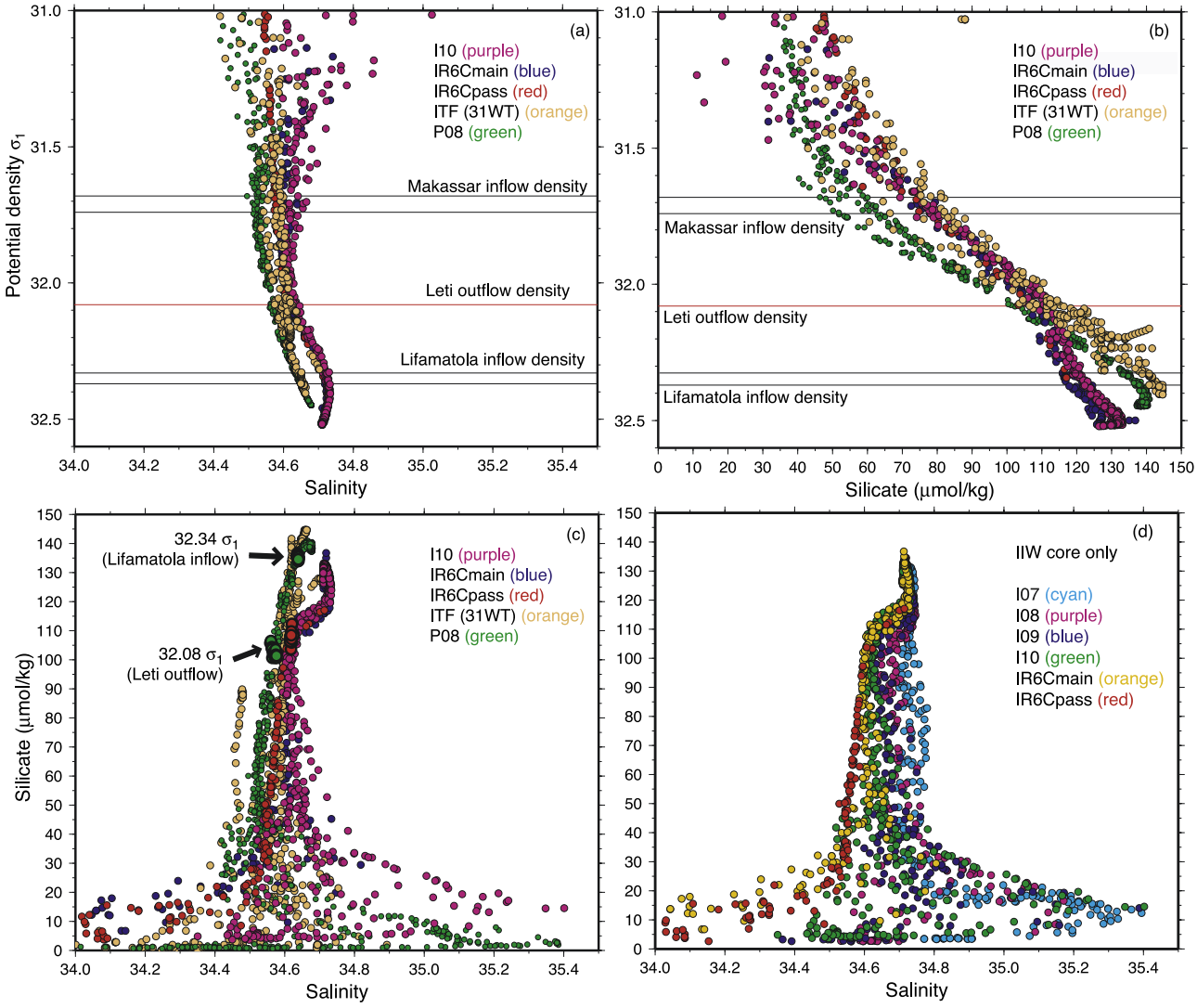

Figure 13. (a–c) Salinity, silicate (μmol/kg), and potential density σ_1 through the Indonesian Passages. Densities marked in Figures 13a and 13b correspond to the approximate sill density at the indicated passages. In Figure 13c, isopycnal properties at the marked densities, associated with the Lifamatola inflow and Leti outflow, are indicated as large symbols (green for P08 and red for IR6C at the Indonesian Throughflow exit). (d) Silicate and salinity at the SEC stations (red stations in Figure 5, used in Figure 12).

(SEISAMW), overlying a highly stratified layer (yellows and oranges in Figure 14). (SEISAMW is the densest subducted water in the Indian Ocean, originating south of Australia.) *McCarthy and Talley* [1999] map Q in the SEISAMW layer and above, showing that the transition from the subtropical low Q to tropical β-domination coincides with the latitude of the SEC. The Q transition shifts southward with increasing density and depth, in accord with the well-known poleward shift of the subtropical gyre with increasing depth [*Reid*, 1994, 1997, 2003; *Young and Rhines*, 1982].

[46] The confinement of the AAIW salinity minimum to the subtropics and separation from IIW is clarified in the Q distribution, shown by *McCarthy and Talley* [1999] for the neutral surface $\gamma^n = 27.35$. AAIW lies in a high Q regime of the subtropical gyre, separated by a zonal front in Q from the lower values of the tropics. Comparing the vertical sections of salinity and potential vorticity (Figures 2 and 14), the AAIW salinity minimum lies at the base of a very high Q layer, which marks the pycnocline beneath the layer of low Q SEISAMW. The IIW lies north of the Q front, within the completely β-dominated potential vorticity regime.

[47] Assuming that potential vorticity is nearly conserved along flow paths, the potential vorticity distributions here and in the work by *McCarthy and Talley* [1999] show that, once established as a westward flow at a single latitude from the surface down to the sill depth of Timor Passage (12°S), the SEC should remain vertically coherent and zonal. Wind forcing across the Indian Ocean creates Sverdrup transport that might shift the SEC across potential vorticity contours. However, the SEC latitude is low enough that the wind

Table 4. Zonal Transport of Indonesian Intermediate Water From WOCE Section Data

WOCE Section, Stations Used for SEC Transport	Isopycnal Layers	Volume Transport, Sv, With *Reid* [2003] Reference Velocities	Volume Transport, Sv, With Zero Velocity at Bottom	Volume Transport, Sv, With SADCP Reference Velocities	Volume Transport, Sv, With LADCP Reference Velocities
IR6C (116°E), 7–19	surface to 31.0σ_1	· · ·	−27.6	· · ·	· · ·
IR6C (116°E), 7–19	31.0–31.5σ_1	· · ·	−4.9	· · ·	· · ·
IR6C (116°E), 7–19	31.5–32.2σ_1	· · ·	−9.9	· · ·	· · ·
I10 (110°E), 1056–1061 (1056–1069)[a]	surface to 31.0σ_1	−9.8 (−3.3)[a]	−12.1 (+5.6)[a]	−7.0 (−23.1)[a]	−8.1 (+10.1)[a]
I10 (110°E), 1056–1061 (1056–1069)[a]	31.0–31.5σ_1	−2.1 (+0.4)[a]	−3.6 (+5.0)[a]	−1.1 (−13.6)[a]	−1.8 (+7.7)[a]
I10 (110°E), 1056–1061 (1056–1069)[a]	31.5–32.2σ_1	−4.3 (−8.5)[a]	−11.2 (+11.4)[a]	+3.3 (−68.4)[a]	−0.3 (+24.0)[a]
I9 (95°E), 180–191,[b] 180–183 (180–187)[a]	surface to 31.0σ_1	−16.7[b] (−11.7)[a]	−14.5[b] (−10.1)[a]	−12.5[b] (−10.2)[a]	−11.9[b] (−6.8)[a]
I9 (95°E), 180–191,[b] 180–183 (180–187)[a]	31.0–31.5σ_1	−2.2 (0.2)[a]	−2.2 (−0.9)[a]	−2.4 (−1.2)[a]	−2.8 (+1.4)[a]
I9 (95°E), 180–191,[b] 180–183 (180–187)[a]	31.5–32.2σ_1	−6.9 (−0.4)[a]	−9.3 (+1.7)[a]	−4.5 (+0.5)[a]	−4.7 (+11.5)[a]
I8 (80°E), 327–333	surface to 31.0σ_1	−9.8	−8.8	−9.4	−10.2
I8 (80°E), 327–333	31.0–31.5σ_1	−1.1	−0.4	−1.5	−2.1
I8 (80°E), 327–333	31.5–32.2σ_1	−3.4	−0.5	−2.7	−5.0
I7 (55°E), 719–725 (716–725)[a]	surface to 31.0σ_1	−3.3 (−12.8)[a]	−11.7 (−22.9)[a]	−9.1 (−19.0)[a]	−3.4 (−8.9)[a]
I7 (55°E), 719–725 (716–725)[a]	31.0–31.5σ_1	−7.8 (−10.3)[a]	−5.4 (−11.8)[a]	−2.9 (−7.6)[a]	+3.0 (+2.6)[a]
I7 (55°E), 719–725 (716–725)[a]	31.5–32.2σ_1	−13.8 (−14.8)[a]	−8.5 (−17.5)[a]	+2.2 (−2.0)[a]	+20.0 (+28.4)[a]

[a]All stations with silica/salinity anomaly, including both westward and eastward flow.
[b]Surface layer only.

stress curl forcing produces only a small change in latitude. It has been shown that the SEC transport is associated with the actual throughflow transport augmented by Sverdrup transport [*Godfrey and Golding*, 1981; *Godfrey*, 1989; *Hirst and Godfrey*, 1993]. In *McCreary et al.*'s [1993] wind-forced 2.5-layer model, the total transport of nearly all of the throughflow moved directly westward across the Indian Ocean.

[48] The penetration of the SEC to great depth is a general feature of all tropical oceans [*Talley and Johnson*, 1994], as modeled by *Nakano and Suginohara* [2002]. Again the zonality of the deep SEC must be associated with the zonality of the Q distribution, broken only below the depth of the mid-ocean ridges [*McCarthy and Talley*, 1999]. On the other hand, it seems puzzling that the upper ocean SEC down through the IIW coincides in latitude with the deep SEC. Since the ITW and IIW portions of the SEC originate in the same passages exiting the Indonesian seas, they should track each other precisely across the Indian Ocean given the zonality of potential vorticity at all depths at this latitude. However, the deeper SEC, marked by meridional salinity and silica fronts, is below the passage depths. If controlled by the equatorial dynamics of *Nakano and Suginohara* [2002], for instance, the SEC latitude at depth would be set by the meridional scale of the equatorial waves that fan outward and downward from the equator, but it is actually very vertical.

6. Velocity and Transport of the SEC (ITW and IIW)

[49] A key question for global budgets is the transport of ITW and IIW waters westward from the Indonesian seas. In the eastern Indian Ocean, *Quadfasel et al.* [1996] estimated a transport of 9 Sv in the upper 470 m of the SEC. At 80°E (I8), in the SEC between 10 and 14°S, *Talley and Baringer* [1997] found a westward geostrophic transport of 6 Sv (21 Sv) in the top 100 m (1500 m), relative to the bottom. Using shipboard ADCP, *Hacker et al.* [1998] obtained SEC transports for the top 275 m of about 13 Sv at 80°E and 10 Sv at 95°E. Using an inverse model with Indian Ocean WOCE data, *Ganachaud et al.* [2000] calculate a net transport of −15±5 Sv entering from the Indonesian seas. Using the WOCE sections, *Gordon et al.* [1997] determined the percentage of ITW in the upper 400 m of the SEC, and estimated westward transports of 4–6 Sv at 95°E, 11–12 Sv at 80°E, and 6–10 Sv at 55°E (relative to 3000 dbar). *Gordon et al.* [1997] showed dilution of the ITW component of the SEC from greater than 90% in the eastern Indian Ocean to 50–60% in the western Indian Ocean. The same sections are used here, but with different reference levels, latitude ranges and vertical intervals to– include the deeper IIW that is clearly of throughflow origin.

[50] Our final estimates (Table 4), discussed in the next paragraphs, are somewhat higher than expected from direct measurements in the Indonesian Straits. We note that the SEC transports obtained in the open Indian Ocean are not directly comparable to the transport through the Indonesian seas because of entrainment/detrainment, isopycnal/diapycnal mixing, and time dependence.

[51] Geostrophic velocities are calculated for each station pair on the meridional WOCE sections. We use several different reference velocity choices: zero bottom velocity, *Reid*'s [2003] reference velocities for each of the station pairs, and reference velocities based on the ADCP direct measurements. *Reid* [2003] obtained bottom reference velocities by balancing transports on the Indian Ocean one-

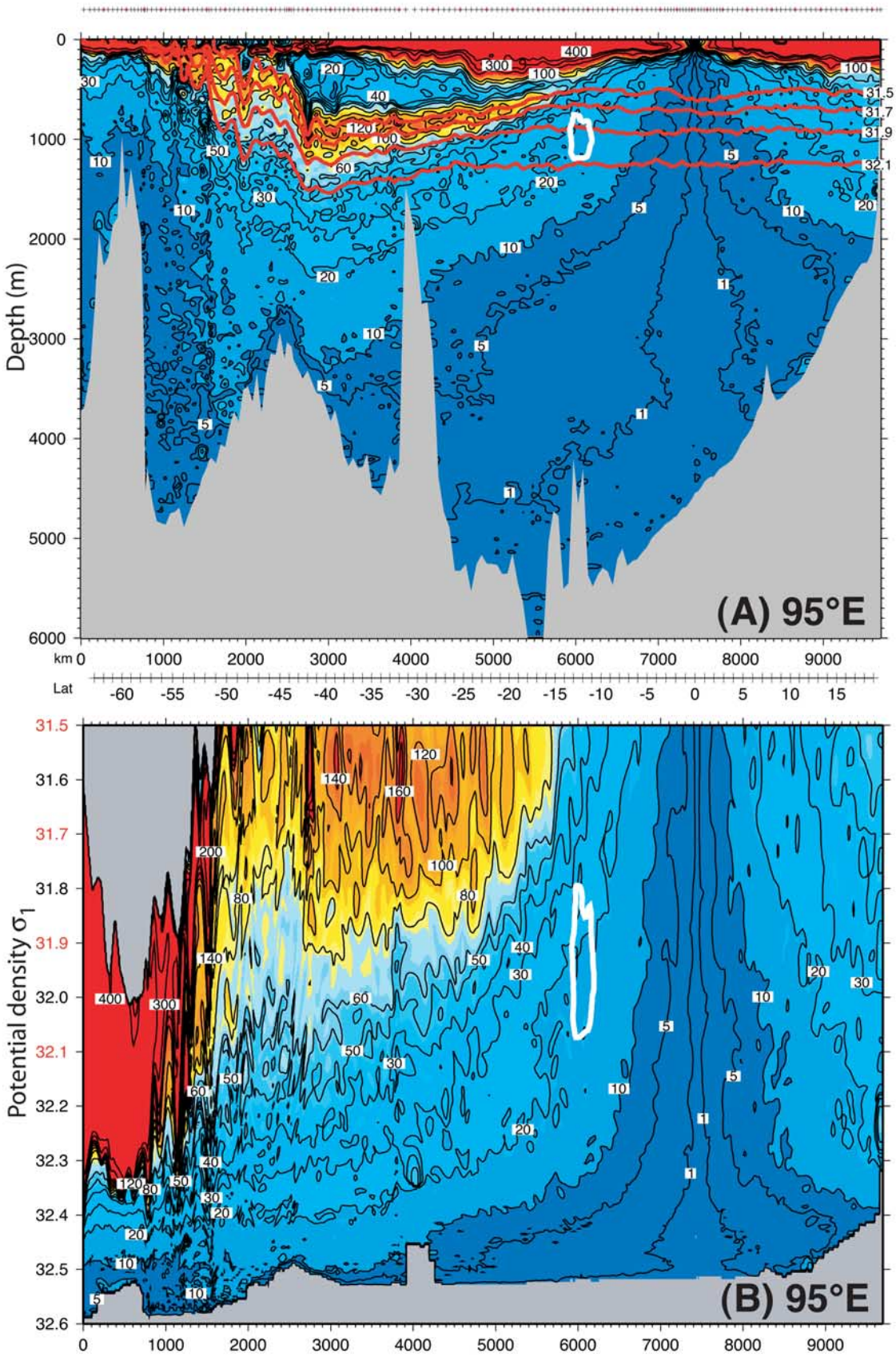

Figure 14. Absolute value of the isopycnic potential vorticity ($\times 10^{-14}$ cm^{-1} s^{-1}) along 95°E (I9), as a function of (a) depth and (b) potential density σ_1. Red curves in Figure 14a are the isopycnals 31.5, 31.7, 31.9, and 32.1 σ_1. The white contour in both panels is the IIW salinity minimum (S = 34.64 from Figure 2).

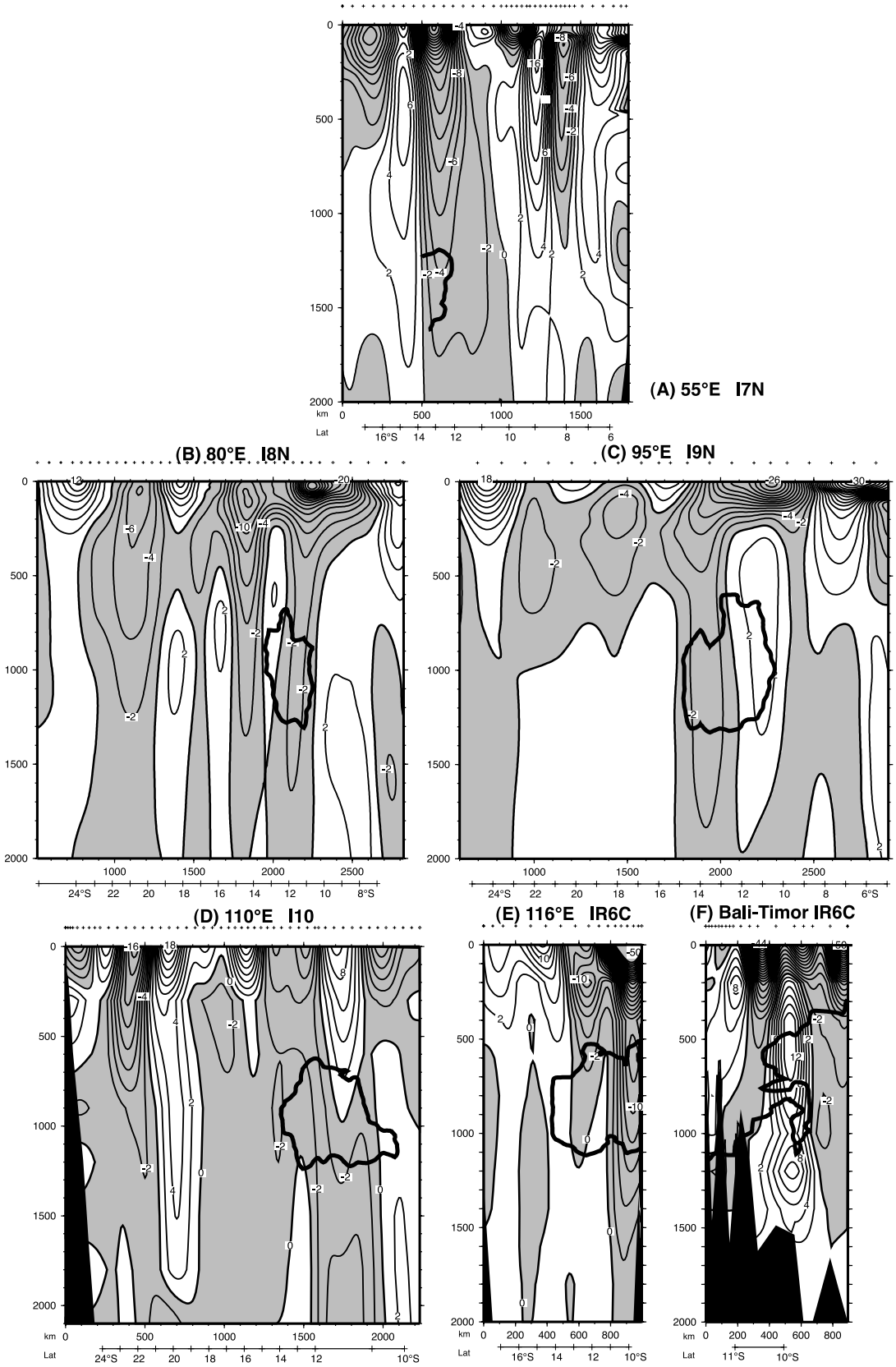

Figure 15. Zonal geostrophic velocities with *Reid* [2003] reference velocities for I7, I8, I9, and I10; bottom reference of 0 cm/s for IR6C. Velocities were smoothed horizontally using a Gaussian filter with 100 km half width. Contours for (a) 55°E (I7), (b) 80°E (I8), (c) 95°E (I9), (d) 110°E (I10), (e) 116°E (IR6C), and (f) Bali-Timor Passage (IR6C). Heavy solid contours are the IIW salinity minimum indicators from Figure 5.

time WOCE sections, considering property distributions on isopycnals throughout the Indian Ocean with all available high-quality data; his reference velocities are therefore similar to those that would be obtained through a formal inverse. To reference velocities to the underway shipboard Acoustic Doppler Current Profiler (SADCP) and the lowered ADCP (LADCP), ADCP transports are calculated over the interval 30–250 dbar (SADCP) or 60–240 dbar (LADCP). A bottom reference velocity is then calculated so that the geostrophic transport matches the ADCP transport over the same shallow depth range.

[52] After examining velocities and transports calculated in each of these ways, we present the geostrophic velocity sections (Figure 15) using *Reid*'s [2003] reference velocities. IR6C is presented relative to a bottom zero velocity since Reid did not use that section. We truncate the geostrophic velocity sections equatorward of 5°S where the values become extremely large.

[53] Like most such sections, the geostrophic velocities are vertically banded, much more than the property distributions. There are several bands of westward flow on each section. A salinity contour from Figure 6 indicating the IIW core is included on all sections except the easternmost. We identify the SEC as the westward band including the IIW, on the basis of salinity and silica anomalies (Figure 12). The SEC is surface intensified, exceeding 30 cm/s on all sections except at 110°E, with strongest velocities on the easternmost sections. Westward flow through the IIW salinity minimum is much smaller, 1 to 2 cm/s.

[54] Like the westward bands, eastward bands are found throughout the sections. At 95°E (I9) and 110°E (I10), the IIW extends into adjacent eastward flow, which we consider to be a local eddy of the SEC. The eastward flow at I7, I8, and I9 at 8° to 10°S is more robust, and is marked by a separate salinity minimum at the IIW level that is weaker than the main IIW salinity minimum; we identify this as a "recirculation" of the SEC, although it could perhaps be best thought of as local eddying from the SEC [*Hacker et al.*, 1998]. The salinity of this recirculated IIW increases toward the west.

[55] Transports were integrated from south to north in isopycnal layers in the SEC (Table 4). The layers were chosen to correspond to the ITW (surface to $31.0\sigma_1$), the salinity maximum layer ($31.0–31.5\sigma_1$), and IIW ($31.5–32.2\sigma_1$). The SEC latitude range is based on the silica-salinity anomaly structure associated with westward flow (Figure 12 and Table 3). The SEC is embedded, especially on I7, I8 and I9, in larger-scale westward flow that includes the northern side of the subtropical gyre. All sections have reversing circulations, so the details of SEC transports are difficult to sort out. At 116°E (IR6C), transport is westward throughout so all stations are used; in Table 4, transports are listed relative to both the bottom and 2000 dbar in the absence of *Reid* [2003] reference velocities. At 110°E (I10), an eddy affected the IIW salinity minimum, recirculating IIW back to the east. Therefore the transport is computed for just the westward flow on the southern side of the closed IIW salinity contour (stations 1056–1061). At 95°E (I9), the subsurface eddy described for the geostrophic velocity (Figure 15c) also creates eastward flow on the north side of the IIW; SEC transports are calculated for the three layers only where the flow is westward (stations listed in Table 4). At 80°E (I8), the SEC westward transport is clearer than on the adjacent sections; westward flow at 15°S is also observed, but is south of the IIW's silica anomaly. At 55°E (I7), a large eddy is centered at 14°S, south of the SEC; it is presumed here that the eastward flow is returned by westward flow, and so the SEC westward transport is calculated only for stations north of the balancing westward flow (for stations 719–725 instead of 716–725).

[56] The transport estimates vary widely depending on reference velocity choice. (They vary even more if the eastward flows dyed with the salinity/silica anomaly are included.) The LADCP-referenced estimates are inconsistent, likely because of the lack of temporal averaging of vigorous ageostrophic flow. For I10, *Sprintall et al.* [2002] suggest that an ageostrophic cyclostrophic flow may contribute to the difference in LADCP and geostrophic transport estimates. IR6C (116°E), calculated either relative to the bottom or to 2000 dbar (not listed), has much larger westward transport than the remaining sections, resulting mainly from the large surface layer transport estimate. I8 (80°E) transports are on the low side in each layer compared with I10 and I9.

[57] The surface layer transport at I8, I9 and I10, referenced to *Reid*'s [2003] bottom velocity, is −10 to −17 Sv. The salinity maximum (second layer) transport is smaller: −1 to −2 Sv. The IIW transport is −3 to −7 Sv. The overall westward transport in these three layers is thus −14 to −26 Sv. This is similar to *Ganachaud et al.*'s [2000] inverse estimate. The *Vranes et al.* [2002] observation of about 10Sv flowing through Makassar Strait matches both our open ocean upper layer transport and the sum of upper ocean transports out of the Indonesian seas through Timor Passage and Lombok and Ombai Straits [*Hautala et al.*, 2001]. The deeper open ocean transports could be at least partially balanced by the inflow through Lifamatola Strait, currently being measured [*Sprintall et al.*, 2004]. The ITF component of the open ocean SEC transports becomes more diluted to the west, because of eddies and associated mixing, as dealt with by *Gordon et al.* [1997]. The ITF properties thus influence a greater area of the Indian Ocean than just the SEC itself, and the calculated transports within the narrowly defined core include an increasing fraction of non-ITF water toward the west.

[58] Sensitivity of the transports to reference level choice is small for the IIW and salinity maximum layers at I8, I9, and I10: estimates fall in the broad range already quoted regardless of referencing methods. However, the IIW transport is more sensitive to reference velocity choice, with an overall range of −11 to +3Sv depending on method. At this depth, the choice made by *Reid* [2003] leads to more consistent estimates from section to section. We prefer the Reid estimate since his choices also conserve mass in large boxes delineated by hydrographic sections, unlike the other more arbitrary (bottom reference) or instantaneous (ADCP) choice.

[59] Robustness of the IIW transport is also apparent from calculations from repeated sections at IR6C and I10, just west of the Indonesian outflow [*Wijffels et al.*, 2002; *Sprintall et al.*, 2002]. At IR6C, transports in the layer 31.5 to $32.2\sigma_1$ were −2.9 Sv in August 1989 and −3.0 Sv

Table 5. Transport Estimates and Budgets[a]

Location	Lifamatola Strait	Dewakang Sill	Lombok Strait	Savu and Sumba Straits (Ombai)	Leti Strait	Sum (Flux Convergence)
Depth, m	1940	650	300	900	1250	···
Hydrographic station	Indopac, 1.8°S, 126.9°E, 8/25/76	Arlindo, 2.8°S, 118.7°E, 8/11/93 and 2/23/94	Arlindo, 7.8°S, 116.8°E, 1/28/94	IR6C 26, 10.5°S, 120.4°E, 8/21/89	Indopac, 7.6°S, 127.8°E, 8/27/76	···
Maximum potential density σ_1 at sill	32.33 σ_1	31.68 σ_1	30.61 σ_1	32.08 σ_1	32.08 σ_1	···
Citation for volume transport	*Fieux et al.* [1994]	*Vranes et al.* [2002]	*Murray and Arief* [1990]	*Hautala et al.* [2001]; *Molcard et al.* [2001]	*Molcard et al.* [1996]	···
Observed volume transport, Sv	−3 to −5	−9 to −10	2 to 4	4 to 5	4 to 5	···
Adjusted volume ransport, Sv	−3	−9	3.6	4	4.4	0
Mean potential temperature, °C	7.0	13.0	18.6	10.8	8.9	···
Heat transport, W	-0.9×10^{14}	-4.8×10^{14}	2.8×10^{14}	1.8×10^{14}	1.6×10^{14}	0.4×10^{14}
Mean salinity	34.59	34.48	34.43	34.47	34.56	···
Freshwater transport relative to 34.5 psu, kg/s	8.5×10^{6}	-5.8×10^{6}	7.8×10^{6}	3.7×10^{6}	-7.4×10^{6}	6.7×10^{6}
Mean oxygen, μmol/kg	116	125	146	109	110	···
Oxygen transport, μmol/s	-3.6×10^{11}	-11.5×10^{11}	5.4×10^{11}	4.5×10^{11}	4.9×10^{11}	-0.2×10^{11}
Mean silica, μmol/kg	85	28	32	50	71	···
Silica transport, μmol/s	-2.6×10^{11}	-2.6×10^{11}	1.2×10^{11}	2.1×10^{11}	3.2×10^{11}	1.2×10^{11}

[a]Positive sign indicates flux out of the Indonesian Seas. Italicized freshwater and heat transports are relative to 34.5 psu and 0°C, so are useful only when summed.

in February 1992 relative to 2000 dbar. In 1995, three occupations of I10, also known as IR6, yielded −1.4 Sv (April), −9.8 Sv (September), and −3.2 Sv (November), all relative to the bottom. The higher September transport reflects the expected seasonal maximum in the throughflow [*Wyrtki*, 1961; *Meyers et al.*, 1995; *Fieux et al.*, 1996b; *Meyers*, 1996] and thus perhaps seasonal variability in IIW, as well as the presence of an energetic mesoscale anticyclonic eddy centered around 13°S at the time of the survey [*Sprintall et al.*, 2002].

7. Source of IIW in the Indonesian Seas

[60] To what extent do the low-salinity and high-silica signatures of IIW in the Indian Ocean arise from Pacific waters that are vigorously mixed in the Indonesian seas, or do they need an enhancement or input of Indian water within the seas? We approach this mainly with flux budgets (section 7.3 and Table 5), to see the extent to which inflowing property transports match outflowing transports. That is, although the outflowing vertical profiles differ significantly from the inflowing because of very strong diapycnal mixing, the total integrated property transports can change only if there are external sources. Although the direct transport measurements we use are not ideal as they cover different time periods, they yield reasonable estimates of heating, freshening, increasing silica, and oxygen consumption rates in the Indonesian seas. Conversely, comparison with established surface and in situ fluxes allows us to tune the transports somewhat.

[61] We begin by briefly examining property distributions on isopycnals characterizing the deeper part of the throughflow (see Figure 17 below), vertical profiles (Figures 12 and 16), and the vertical sections constructed from the Indian to the Pacific (Figures 3 and 11). Silica coverage is sparse, and is absent in the western Indonesian seas and Makassar Strait (Figure 17). Oxygen data are available throughout the region and are a useful constraint on the silica and salinity budgets, since oxygen must be consumed overall. The chosen isopycnals represent IIW (31.96 σ_1), the top of the IIW (31.5 σ_1), and the bottom water in the Banda Sea (32.22 σ_1). The maximum bottom density in the Indonesian seas is $32.25\sigma_1$ whereas the highest density at Lifamatola Strait is $32.33\sigma_1$. Diapycnal mixing at Lifamatola strait along with net heating and precipitation within the Indonesian seas combine to eliminate the highest inflow density [*Van Bennekom*, 1988; *Gordon et al.*, 2003].

7.1. Salinity Distribution

[62] The effects of mixing and local sources in the Indonesian seas on salinity have been characterized by *Hautala et al.* [1996], *Ffield and Gordon* [1992, 1996], and *Gordon et al.* [2003], using station profiles, isopycnal maps, and advection-diffusion models. Diapycnal salinity gradients are dramatically reduced within the Indonesian seas (Figures 3 and 16). Jumps occur at Lifamatola and Leti Straits, indicating their importance to diapycnal mixing [*Van Bennekom*, 1988; *Van Bennekom et al.*, 1988; *Gordon et al.*, 2003]. Salinity increases overall from the Pacific to the Indian Ocean on all isopycnals except in the uppermost layer (which contains a salinity maximum in the Pacific) (Figures 3b and 16). Since there is net precipitation in the Indonesian seas, these increases result from diapycnal mixing [e.g., *Ffield and Gordon*, 1992; *Hautala et al.*, 1996].

[63] In the lower thermocline ($31.5\sigma_1$), fresher North Pacific water masses enter primarily through Makassar Strait and the saltier South Pacific waters enter via the deeper Lifamatola Strait, leading to a salinity gradient across the Banda Sea. The isolated high salinity within the Seram Sea is due to downward mixing from the South Pacific salinity maximum [*Ilahude and Gordon*, 1996]. Isopycnal spreading from the Pacific was hypothesized by *Hautala et al.* [1996] to account for the lower thermocline (25.8–27 σ_θ; $30.1-31.5\sigma_1$) salinity distribution in the Banda Sea (Figure 17d), with diapycnal mixing

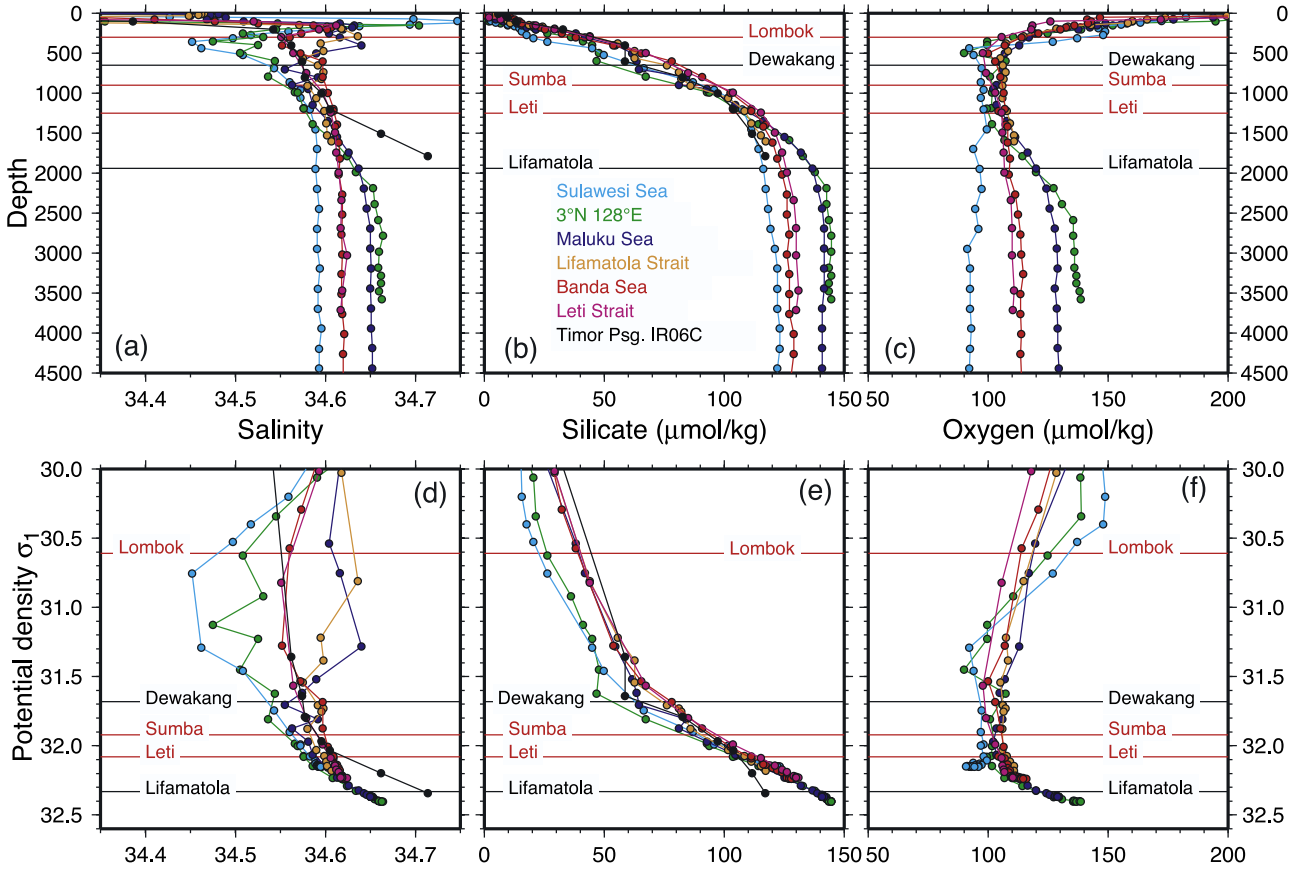

Figure 16. Salinity, silicate (μmol/kg) and oxygen (μmol/kg) as a function of (a–c) depth and (d–f) potential density σ_1. All stations except at Timor Passage are from the 1976 Indopac expedition. The Timor Passage station is from WOCE IR6C. All stations except the Sulawesi station are along the synthetic section (shaded in Figure 1; used in Figures 3 and 11).

above and below creating the isohaline Banda Sea vertical profile (e.g., Figures 3b and 16). On the other hand, silica and oxygen, discussed below, indicate that diapycnal mixing within the lower thermocline should be as strong as above and below.

[64] In the IIW core at $31.96\sigma_1$ (950–1000 m, Figure 17b), salinity increases to the east across the Banda Sea (Figure 17e) [also *Hautala et al.*, 1996]. Such high salinities are not found at this density upstream in the Pacific, but lie deeper in the water column (e.g., $32.22\sigma_1$ in Figure 17f). Thus the general increase in salinity at $31.96\sigma_1$ could be due to diapycnal mixing with the underlying waters as they spill across Lifamatola Strait. In the Flores Sea in the west, low salinities at $31.96\sigma_1$ are likely due to mixing with the overlying fresher water from Makassar Strait (e.g., $31.5\sigma_1$ in Figure 17d), and also the voluminous freshwater input from river runoff in this region [*Wyrtki*, 1961]. The fresher Flores Sea Water enters the southern Banda Basin and Savu Sea [*Molcard et al.*, 2001].

[65] Is an input of saline Indian Ocean water into the Indonesian seas, suggested by *Hautala et al.* [1996] and *Wyrtki* [1961], required to produce the observed IIW properties? The densest waters in Timor Trench come from the Indian Ocean, as reflected in their high salinity (Figure 17f). The high salinity in the Aru and Seram basins at $31.96\sigma_1$ (Figure 17e) could suggest an input of saltier Indian Ocean deep water [*Wyrtki*, 1961]. However, the high Aru and Seram salinity could also come from diapycnal mixing of the higher salinity, densest Pacific waters (Figure 17f). There is little evidence for eastward flow in this depth range from the Indian Ocean, except for a current meter at 1040 m depth on the western sill of the Timor Trench that had brief periods of small eastward velocities [*Molcard et al.*, 1996]. Water mass analysis and a few current profiles on the western Timor sill also suggest westward flow at this depth and above, although eastward flow is evident below 1200 m to the bottom in the current profiles [*Cresswell et al.*, 1993; *Fieux et al.*, 1994].

[66] Shallower Indian Ocean waters (400–800 m) also have high salinity (~34.68) in the salinity maximum layer (North Indian Intermediate Water) (Figures 6f and 17d). However, we see no evidence of this high salinity entering the Banda Sea, and thus it is probably not involved in IIW formation. This is consistent with current meter and CTD data from Ombai Strait [*Molcard et al.*, 2001]. All of the ITF water column entering the Indian Ocean on WOCE section IR6C is relatively fresh (Figure 7). Once the ITF waters enter the Indian Ocean, the vertical separation between the low-salinity ITF and IIW is due to interaction with this salinity maximum water.

7.2. Silica and Oxygen Distributions

[67] Silica is enhanced in the IIW layer in the Indonesian seas (Figures 17h and 11). This enhancement reaches far

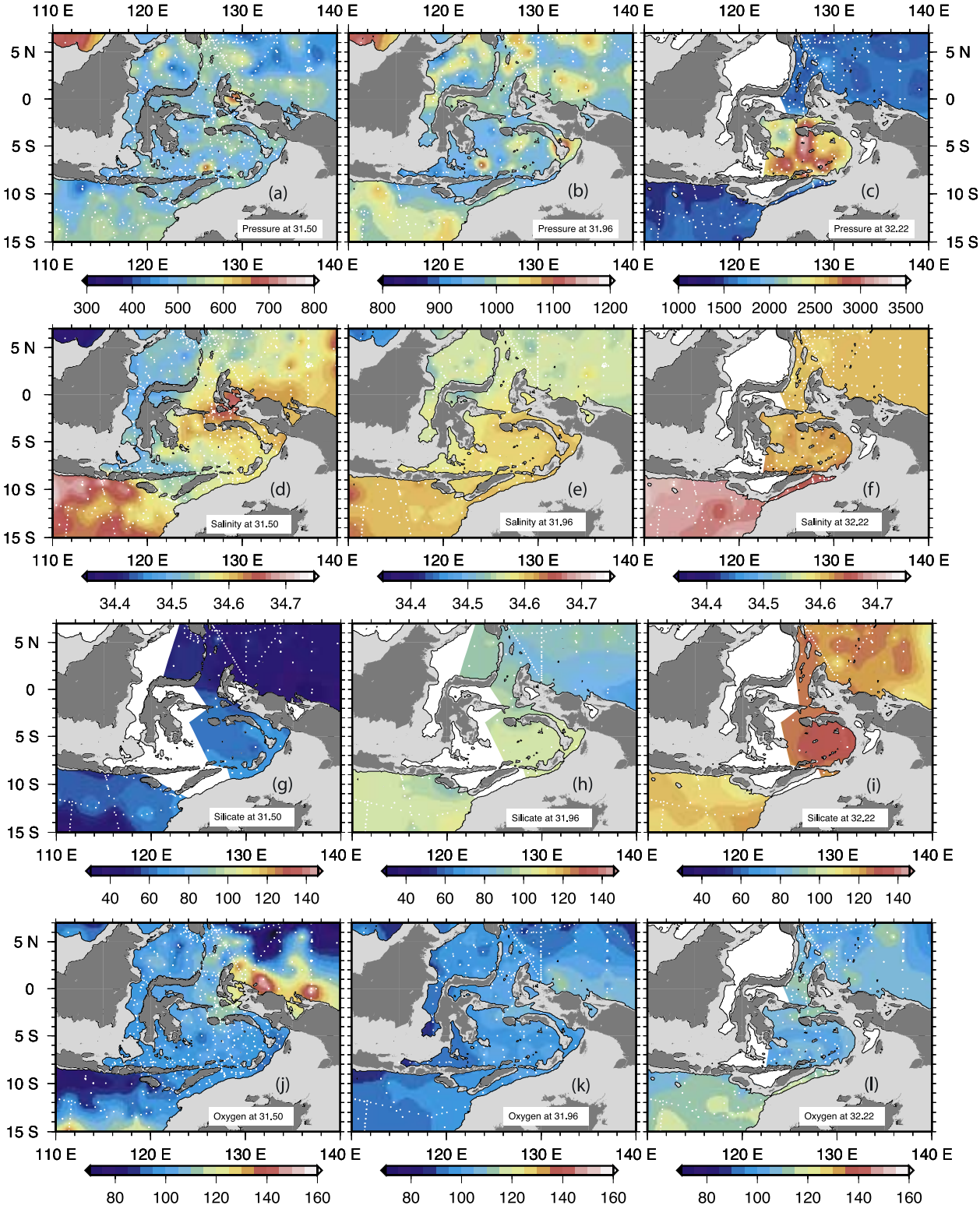

Figure 17. (a–c) Pressure (dbar), (d–f) salinity, (g–i) silica (μmol/kg), and (j–l) oxygen (μmol/kg) at 31.50, 31.96, and 32.22σ_1 (left to right), with 500, 1000, and 1500 m isobaths, respectively. Stations are shown as white dots. Regions with no data are whited out.

up into the water column and reaches well into the Indian Ocean, as evidenced in the upward doming of silica isolines in Figure 11b. Higher silica is also clear on the thermocline isopycnal 31.5σ_1 (Figure 17g), with highest values arrayed around the Aru Basin in the east. The enhanced Indonesian silica is easily apparent on vertical profiles, especially when plotted versus density (Figures 11b and 16e).

[68] Silica at the near-bottom density in the Banda Sea (Figure 17i) is the highest anywhere in this region. However, from the vertical profiles, it is clear that higher silica sits at the same depth just north of Lifamatola Strait (Figure 16b), albeit at slightly higher density (Figure 16e). As argued for salinity, when the densest water at Lifamatola Strait cascades over the sill and disappears, its higher silica content must be mixed into the water column, and certainly into the densities found near the Banda Sea bottom. Longer residence times of the Banda Sea bottom waters increase deep silica through bottom dissolution, but this does not necessarily mean that there is a net flux of silica into the water column in the Indonesian seas since the source of bottom silica could be entirely due to particle flux from the surface waters.

[69] The flux calculations in section 7.3 do however suggest an additional input of silica. *Van Bennekom* [1988] and *Van Bennekom and Muchtar* [1988] inferred additional silica sources in the bottom sediments in the deep Seram and Aru basins. Further, on the basis of the lateral distribution of silica, *Van Bennekom et al.* [1988] suggested an anticyclonic circulation in the Banda Sea, sourced by Indian Ocean deep water overflowing into the Timor Trench [*Wyrtki*, 1961], extending upward into the intermediate waters at 750 m. However, as discussed above for salinity distributions, it is not clear that such a back flow into the Indonesian seas is required to produce the observed distributions, given the possibility of diapycnal mixing of pure Pacific waters with a limited and reasonable internal source of silica (and freshwater).

[70] Oxygen consumption is a useful constraint in the budgets (section 7.3). Since most of the water column does not outcrop anywhere in this tropical region, oxygen can only be consumed or redistributed through mixing. On the isopycnals in the lower thermocline and below (Figures 16, 17j, 17k, and 17l), the high-oxygen source for the Indonesian seas is the South Pacific water arriving in the New Guinea Coastal undercurrent. The low-oxygen source is the North Pacific water entering through Makassar Strait, as noted by *Hautala et al.* [1996], who showed that the IIW portion of the water column, as well as the densities of the deeper Indonesian sills, lie within the oxygen minimum layer of the Pacific. Just as with silica, when the Pacific waters spill over Lifamatola Strait, the higher oxygen of the densest water at the sill mixes upward into the oxygen minimum (Figures 17c and 17f). Likewise, diapycnal mixing of the oxygen minimum decreases the upper layer oxygen.

7.3. Flux Divergences

[71] Convergence of heat, freshwater, silica and oxygen fluxes are computed for the internal Indonesian seas, using direct estimates of the transports and individual hydrographic profiles for the five major passages: inflow from the Pacific at Dewakang (Makassar) and Lifamatola, and outflow at Lombok, Ombai (Savu and Sumba) and Leti Straits (Table 5). An accurate estimate of property flux requires simultaneous velocity and property observations:

$$\mathrm{F} = \int\int \rho v C \, dxdz \qquad (2)$$

where v is velocity, C is the property concentration, and integration is over the cross section of the strait. For freshwater flux, C is the quantity $(1 - S/S_o)$ where S_o is any arbitrary constant salinity, chosen here as 34.5 [*Wijffels*, 2001; L. D. Talley et al., manuscript in preparation, 2005]. By estimating the fluxes at the major inflow and outflow straits and requiring the inflows and outflows to balance, (2) yields the flux divergence of each property C over the Indonesian seas, which should be balanced by local sources and sinks of C.

[72] Transport estimates for the passages do not include concurrent property time series, and some do not have full vertical resolution. Therefore we compute only a crude balance for each strait:

$$F \simeq V\langle \rho C \rangle \qquad (3)$$

where V is total volume transport and brackets indicate the mean value.

[73] Our initial choice of volume transports for the five major straits was -9 Sv and -3 Sv for Dewakang and Lifamatola, respectively, and 3 Sv, 4 Sv and 5 Sv for Lombok, Ombai (Savu/Sumba) and Leti Straits, respectively (Table 5, including published sources; see *Molcard et al.* [2001] and review by *Gordon et al.* [2003]). Negative (positive) values are fluxes into (out of) the internal seas. These are within the observed range for each strait, and are chosen to be mass balanced. After testing sensitivity of the property flux divergences to variations of these transports within their observed ranges and comparing the flux divergences with rough estimates of expected sources and sinks, we settled on a slightly adjusted final set of transports (Table 5). We also varied the transport assumptions widely (Table 6) to understand the sensitivity of the implied flux divergences to the presence of shallow and deep inflows and outflows.

[74] Hydrographic profiles were taken from the Indopac, WOCE IR6C, and Arlindo data sets. WOCE IR6C and Indopac have both silica and oxygen; Arlindo has no oxygen or silica. There are no modern silica measurements in Makassar (Dewakang) or Lombok straits. A silica profile from the nearest available station is used for each; the resulting error is small, because silica is low in the upper ocean. Potential temperature, salinity, the quantity $(1-S/S_o)$ for freshwater flux, oxygen, and silica were integrated from the surface to sill depth, to yield their mean values and the bracketed quantity in (3) for the flux. Most profiles were not exactly at the saddle point of the strait. The maximum potential density at each strait (Table 5) was used to set the depth of integration for the nearby station profile.

[75] For comparison, external estimates of net flux of heat and freshwater and of consumption of oxygen were obtained from various sources (Table 6). To convert between total flux divergences and fluxes per unit area, an area and volume of 1.7×10^{12} m^2 and 3.3×10^{15} m^3 for the Indonesian seas was used (depths greater than 50 m). NCEP air-sea heat flux averages 25 to 50 W/m^2. Net precipitation/evaporation from *da Silva et al.* [1994] is 0 to 20 cm/yr. Oxygen consumption has not been estimated in the Indonesian region. Estimates from other regions are as much as 8–10 μmol kg^{-1} yr^{-1} for the surface layer, to about 3 μmol kg^{-1} yr^{-1} at about 300 m depth [*Sonnerup et al.*, 1999; *Jenkins*, 1987] down to 1 to 2 μmol kg^{-1} yr^{-1} at 1000 to 1500 m depth [*Jenkins*, 1987]. Over the volume of the

Table 6. Sensitivity of Indonesian Seas' Net Flux Divergences to Choices of Transports[a]

Volume Transport, Sv, LF, DW, LM, SU, LT	Heat, 10^{15} W	Freshwater, 10^{9} kg/s	Oxygen, 10^{11} μmol/s	Silica, 10^{11} μmol/s
References (see text)	0.05 to 0.08	0.008 to 0.013	−0.3	0.6 to 1.5
Initial choice, 3, 9, 3, 4, 5	0.02	0.004	−0.4	1.5
Molcard et al. [2001], 3, 9, 2, 5, 5	*−0.01*	0.003	−0.8	1.6
Adjusted choice, 3, 9, 3.6, 4.0, 4.4	0.04	0.007	−0.2	1.2
Low oxygen flux, 3, 9, 4.1, 4, 3.9	0.06	0.009	−0.03	1.0
In shallow, out shallow, 0, 12, 12, 0, 0	0.27	0.02	*2.7*	0.50
In shallow, out deep, 0, 12, 0, 6, 6	*−0.16*	*−0.01*	−1.8	4.0
In deep, out shallow, 12, 0, 12, 0, 0	0.57	0.06	*3.6*	*−6.6*
In deep, out deep, 12, 0, 0, 6, 6	0.14	0.03	−0.8	*−3.1*

[a]LF, Lifamatola; DW, Dewakang; LM, Lombok; SU, Savu/Sumba; LT, Leti. Italicized fluxes are the wrong sign compared with physically plausible fluxes, thus eliminating these extreme choices of transport balances from consideration.

Indonesian seas, this yields an oxygen consumption range of 1 to 10×10^{11} μmol/s; we target a value of 3×10^{11} μmol/s, in the middle of the range and a reasonable average for the seas as a whole. Silica flux into the water column of 1 to 2.5 mol m^{-2} yr^{-1} was estimated for the Indonesian seas by *Van Bennekom et al.* [1988], equivalent to 0.6 to 1.5×10^{11} μmol/s over the area of the seas.

[76] Oxygen must be consumed on average during the transit through the Indonesian seas. The net oxygen transport divergence estimated from (3), using the initial choice of strait volume transports, is 4×10^{11} μmol/s (Table 6). This is within the large range of estimates listed above, but somewhat high. Our value is easily reduced to 3×10^{11}μmol/s by assigning a higher transport of 3.6 Sv to the shallow outflow (e.g., Lombok Strait), with a slight decrease in outflow through the deeper straits. This adjustment actually improves the heat and freshwater divergences, as described next.

[77] The Indonesian seas are subject to net precipitation/runoff over evaporation. For our initial choice of transports, we obtain a small net flux divergence of 0.004×10^{9} kg/s (Table 6). If the transports are adjusted as described in the previous paragraph to lower the estimated oxygen consumption rate, the freshwater divergence is 0.007×10^{9} kg/s. Over an area of 1.7×10^{12} m^2, this is a net precipitation rate of 13 cm/yr, which is comparable to observed surface fluxes (Table 6).

[78] Net heating within the Indonesian seas is obvious from surface heat flux maps. Also, the coldest inflow from the Pacific is colder and denser than the coldest water within the seas. The initial choice of strait transports yields a net heating of 0.02×10^{15} W, which is lower than the observed air-sea heat flux. Adjusting the volume transports to yield the lower oxygen consumption rate results in a net heating of 0.04×10^{15} W, or a net surface heat flux of 25 W/m^2, within the observed surface flux range of 25 to 50 W/m^2.

[79] Finally, the Indonesian seas are a source of silica to the water column [*Broecker et al.*, 1986; *Van Bennekom et al.*, 1988]. Silica flux divergence cannot be diagnosed simply by looking at the mean silica value at each strait (Table 5). The silica flux divergence (source within the Indonesian seas), using the initial choice of strait transports, is 1.5×10^{11} μmol/s. Adjusting the strait transports to yield the lower oxygen consumption rate, the silica divergence is reduced to 1.2×10^{11} μmol/s. This is comparable to *Van Bennekom et al.*'s [1988] estimate of 0.6 to 1.5×10^{11} μmol/s.

[80] If there were no net silica source within the Indonesian seas, the mean silica for the deep (Savu and Leti Strait) outflows would average 10 to 15 μmol/kg lower than observed, on the basis of the difference between the inflow and outflow silica transports and a 12 Sv throughput. Comparing with Figure 9b, this is a significant signal, and is in fact similar to the increase in silica on the isopycnal $31.96\sigma_1$ from its source in the Pacific to its value within the Indonesian seas. If there were no net heating, net precipitation minus evaporation, or net oxygen consumption, the average outflow temperature would be 0.8°C lower, salinity would be 0.004 higher, and oxygen would be 2 μmol/kg higher. The buoyancy flux is thus almost entirely due to heating, resulting in an average density reduction of about 0.2 kg/m^3. Thus bulk silica, temperature and density are most affected by internal sources in the Indonesian seas, while salinity and oxygen change only a little. (However, obviously the vertical distribution of all properties changes radically because of the intense vertical mixing within the seas.)

[81] The simplest possible model of Indonesian transports must include both shallow and deep inflows and outflows. All possible combinations of shallow and deep inflows and outflows are tested (Table 6). Looking at the most extreme transport choices in Table 6, the net precipitation and heating eliminate the possibility of exclusively shallow inflow (through Makassar) balanced by exclusively deep outflow, since then the outflow would have to be saltier and colder than the inflow. Net oxygen consumption eliminates the possibility that all outflow is shallow (i.e., through Lombok, with no outflow through Sumba/Savu or Leti). Finally, net silica production eliminates the possibility that all inflow could be deep (e.g., there must be inflow through Makassar). On the other hand, we cannot distinguish the relative importance of Savu, Sumba or Leti Straits for deep outflow, given the crudeness of the flux estimates. If bulk temperature, density and silica changes within the Indonesian seas are to be modeled, external sources of heat and silica must also be included; freshwater changes are small.

8. Summary

[82] In the Indian Ocean, the flow in the zonal South Equatorial Current, located between 11°S and 14°S, includes two distinct low-salinity layers from the Indonesian Throughflow. The upper layer is the Indonesian Throughflow Water (ITW), which has been the focus of many ITF

descriptions and transport studies. Its westward volume transport from previous studies is −5 to −10 Sv [*Gordon et al.*, 1997]. The intermediate depth feature (Indonesian Intermediate Water or IIW) had been previously identified as a vertical salinity minimum and is here also identified as a meridional silica maximum. The westward geostrophic flow identified as IIW on all six meridional Indian Ocean WOCE sections remains remarkably zonal, within 1° latitude of 12°S. The silica signature permits us to define the bottom of the IIW layer on each section, which is particularly useful for the transport estimates of the IIW in the SEC, of −3 to −7 Sv, on the basis of geostrophic velocities using *Reid*'s [2003] reference velocities, and which we compared with transports that we calculated from LADCP velocities. The total westward transport of the SEC in the layers affected by the ITF (ITW, salinity maximum layer, and IIW) is −14 to −26 Sv, which is larger than the actual ITF transport of about 12 Sv, although both estimates have error. A larger mid-ocean transport could easily arise because of local Indian Ocean waters entrained into the SEC.

[83] The SEC is a vertical water mass boundary, extending from the surface to well below the IIW, and to the abyss in the eastern Indian Ocean. We believe that this extreme zonality and the top-to-bottom penetration of the boundary have not been remarked on or emphasized before. In the upper ocean, the ITF waters of the SEC separate waters of strongly subtropical properties (higher oxygen) from tropical waters (low oxygen, higher nutrients). Below the IIW, the SEC persists as a water mass boundary that is apparent in silica. The zonal nature of the SEC is associated with the zonal potential vorticity contours in the tropics. The SEC latitude is apparently set by the maximum meridional potential vorticity gradient in the uppermost ocean, separating the very zonal potential vorticity in the tropics from the more mixed potential vorticity in the subtropical gyre. The strongly barotropic nature of the SEC is puzzling since models show the tropical jets fanning southward and downward [*Nakano and Suginohara*, 2002].

[84] The tropical properties and flows are symmetric about the equator, reflecting eastward flow on the equator and westward flow in the deep SEC south of the equator and in the Bay of Bengal [*Reid*, 2003]. The equatorial symmetry suggests that the westward flow of the ITF waters in the SEC is not simply driven by a pressure difference between the Pacific and Indian oceans, but by tropical dynamics internal to the Indian Ocean. (On the other hand, the transport of waters through the Indonesian passages from the Pacific to the Indian is driven by such a pressure difference, as is the persistently southward Leeuwin Current along the coast of Australia.) A similar tropical structure is found at greater depth in the Pacific and Atlantic oceans [e.g., *Talley and Johnson*, 1994]. We suggest that the nearly exactly zonal penetration of the ITF waters westward across the Indian Ocean is a coincidence of the location of the Savu Strait/Timor Passage with the large-scale tropical potential vorticity field and frontal structure of the Indian Ocean.

[85] Waters in the deeper part of the Indonesian Throughflow jet originate from waters that move from the Pacific to the Indian Ocean through the deepest portions of the Indonesian passages, undergoing strong diapycnal mixing in the Indonesian seas, as has been demonstrated repeatedly before. The deepest pathway that permits intermediate water flow from the Pacific Ocean to the Indian Ocean is through the Maluku Sea into the Banda Sea, via the 1940 m Lifamatola Passage, and then exiting via Leti and Timor Straits (1250 and 1890 m). From the distributions of silica and salinity at intermediate depths in the internal Indonesian seas, we show that the IIW attains most of its characteristics immediately downstream of Lifamatola Strait as a result of diapycnal mixing of the intermediate Pacific Ocean water masses, with a larger contribution from the saltier water masses of the South Pacific found at depth in the Banda basin.

[86] Our new, albeit rough, flux divergence calculations for the Indonesian seas, based on heat, freshwater, oxygen and silica, show the importance of both deep and shallow inflows and outflows; the absence of any one of these four components of flow results in unphysical fluxes. The calculations support a net throughflow of approximately 12 Sv, roughly divided as 9 Sv through the shallow Makassar Strait, 3 Sv through the deep Lifamatola Strait, 3 to 4 Sv out through the shallow Lombok Strait, and 8 to 9 Sv out distributed among the deep Savu, Sumba, and Timor Straits.

[87] **Acknowledgments.** Funding was provided by the National Science Foundation's grant OCE-9413160 supporting collection of WOCE data along I8N (LDT), and grants OCE-0118046 (LDT) and OCE-9818670 (JS) for data analysis. We are grateful to M. Fieux for detailed comments and nonpublic JADE data which were collected through Franco-Indonesian cooperation (PIs Fieux and Ilahude). Gratitude is expressed to the many who collected and processed the WOCE data (http://whpo.ucsd.edu): the principal investigators, chief scientists, captains and crews, Scripps Institution of Oceanography's Oceanographic Data Facility, and Woods Hole Oceanographic Institution.

References

Alford, M. H., M. C. Gregg, and M. Ilyas (1999), Diapycnal mixing in the Banda Sea: Results of the first microstructure measurements in the Indonesian Throughflow, *Geophys. Res. Lett.*, *26*, 2741–2744.

Blanke, B., S. Speich, G. Madec, and K. Doos (2001), A global diagnostic of interocean mass transfers, *J. Phys. Oceanogr.*, *31*, 1623–1632.

Broecker, W. S. (1991), The great ocean conveyor, *Oceanography*, *3*, 79–89.

Broecker, W. S., W. C. Patzert, J. R. Toggweiler, and M. Stuiver (1986), Hydrography, chemistry and radioisotopes in the Southeast Asian basins, *J. Geophys. Res.*, *91*, 14,345–14,354.

Cresswell, G., A. Frische, J. Peterson, and D. Quadfasel (1993), Circulation in the Timor Sea, *J. Geophys. Res.*, *98*, 14,379–14,389.

da Silva, A. M., C. C. Young, and S. Levitus (1994), *Atlas of Surface Marine Data 1994,* vol. 4, *Anomalies of Fresh Water Fluxes*, *NOAA Atlas NESDIS 9*, NOAA, Silver Spring, Md.

Edmond, J. M., S. S. Jacobs, A. L. Gordon, A. W. Mantyla, and R. F. Weiss (1979), Water column anomalies in dissolved silica over opaline pelagic sediments and the origin of the deep silica maximum, *J. Geophys. Res.*, *84*, 7809–7826.

Emery, W. J., and J. Meincke (1986), Global water masses: Summary and review, *Oceanol. Acta*, *9*, 383–391.

Ffield, A., and A. L. Gordon (1992), Vertical mixing in the Indonesian thermocline, *J. Phys. Oceanogr.*, *22*, 184–195.

Ffield, A., and A. Gordon (1996), Tidal mixing signatures in the Indonesian seas, *J. Phys. Oceanogr.*, *26*, 1924–1937.

Fieux, M., C. Andrie, P. Delecluse, A. G. Ilahude, A. Kartavtseff, F. Mantisi, R. Molcard, and J. C. Swallow (1994), Measurements within the Pacific-Indian oceans throughflow region, *Deep Sea Res., Part I*, *41*, 1091–1130.

Fieux, M., C. Andrie, E. Charriaud, A. G. Ilahude, N. Metzl, R. Molcard, and J. C. Swallow (1996a), Hydrological and chlorofluoromethane measurements of the Indonesian throughflow entering the Indian Ocean, *J. Geophys. Res.*, *101*, 12,433–12,454.

Fieux, M., R. Molcard, and A. G. Ilahude (1996b), Geostrophic transport of the Pacific Indian Oceans throughflow, *J. Geophys. Res.*, *101*, 12,421–12,432.

Fine, R. A., R. Lukas, F. D. Bingham, M. J. Warner, and R. H. Gammon (1994), The western equatorial Pacific: A water mass crossroads, *J. Geophys. Res.*, *99*, 25,063–25,080.

Firing, E. (1989), Mean zonal currents below 1500 m near the equator, 159°W, *J. Geophys. Res.*, *94*, 2023–2028.

Ganachaud, A., C. Wunsch, J. Marotzke, and J. Toole (2000), The meridional overturning and large-scale circulation of the Indian Ocean, *J. Geophys. Res.*, *105*, 26,117–26,134.

Godfrey, J. S. (1989), A Sverdrup model of the depth-integrated flow from the world ocean allowing for island circulations, *Geophys. Astrophys. Fluid Dyn.*, *45*, 89–112.

Godfrey, J. S., and T. J. Golding (1981), The Sverdrup relation in the Indian Ocean, and the effect of Pacific-Indian Ocean throughflow on Indian Ocean circulation and on the East Australian Current, *J. Phys. Oceanogr.*, *11*, 771–779.

Gordon, A. L. (1986), Interocean exchange of thermocline water, *J. Geophys. Res.*, *91*, 5037–5046.

Gordon, A. L. (1995), When is appearance reality? A comment on why does the Indonesian Throughflow appear to originate from the North Pacific, *J. Phys. Oceanogr.*, *25*, 1560–1567.

Gordon, A., and R. Fine (1996), Pathways of water between the Pacific and Indian oceans in the Indonesian Seas, *Nature*, *379*, 146–149.

Gordon, A. L., A. Ffield, and A. G. Ilahude (1994), Thermocline of the Flores and Banda seas, *J. Geophys. Res.*, *99*, 18,235–18,242.

Gordon, A. L., S. Ma, D. B. Olson, P. Hacker, A. Ffield, L. D. Talley, D. Wilson, and M. Baringer (1997), Advection and diffusion of Indonesian throughflow water within the Indian Ocean South Equatorial Current, *Geophys. Res. Lett.*, *24*, 2573–2576.

Gordon, A. L., R. D. Susanto, and A. L. Ffield (1999), Throughflow within Makassar Strait, *Geophys. Res. Lett.*, *26*, 3325–3328.

Gordon, A. L., C. F. Giulivi, T. Takahashi, S. Sutherland, J. Morrison, and D. Olson (2002), Bay of Bengal nutrient-rich benthic layer, *Deep Sea Res., Part II*, *49*, 1411–1421.

Gordon, A. L., C. F. Giulivi, and A. G. Ilahude (2003), Deep topographic barriers within the Indonesian seas, *Deep Sea Res., Part II*, *50*, 2205–2228.

Hacker, P., E. Firing, J. Hummon, A. L. Gordon, and J. C. Kindle (1998), Bay of Bengal currents during the northeast monsoon, *Geophys. Res. Lett.*, *25*, 2769–2772.

Hautala, S. L., J. L. Reid, and N. Bray (1996), The distribution and mixing of Pacific water masses in the Indonesian seas, *J. Geophys. Res.*, *101*, 12,375–12,390.

Hautala, S. L., J. Sprintall, J. T. Potemra, J. C. Chong, W. Pandoe, N. Bray, and A. G. Ilahude (2001), Velocity structure and transport of the Indonesian Throughflow in the major straits restricting flow into the Indian Ocean, *J. Geophys. Res.*, *106*, 19,527–19,546.

Hirst, A. C., and J. S. Godfrey (1993), The role of Indonesian throughflow in an global ocean GCM, *J. Phys. Oceanogr.*, *23*, 1057–1086.

Ilahude, A. G., and A. L. Gordon (1996), Thermocline stratification within the Indonesian seas, *J. Geophys. Res.*, *101*, 12,401–12,410.

Jackett, D. R., and T. J. McDougall (1997), A neutral density variable for the world's oceans, *J. Phys. Oceanogr.*, *27*, 237–263.

Jean-Baptiste, P., M. Fieux, and A. G. Ilahude (1997), An eastern Indian Ocean ^{3}He section from Australia to Bali: Evidence for a deep Pacific-Indian throughflow, *Geophys. Res. Lett.*, *24*, 2577–2772.

Jenkins, W. J. (1987), ^{3}H and ^{3}He in the beta triangle: Observations of gyre ventilation and oxygen utilization rates, *J. Phys. Oceanogr.*, *17*, 763–783.

Leetmaa, A., and P. F. Spain (1981), Results from a velocity transect along the equator from 125 to 159°W, *J. Phys. Oceanogr.*, *11*, 1030–1033.

Lukas, R., E. Firing, P. Hacker, P. L. Richardson, C. A. Collins, R. Fine, and R. Gammon (1991), Observations of the Mindanao Current during the Western Equatorial Pacific Ocean Circulation Study, *J. Geophys. Res.*, *96*, 7089–7104.

Luyten, J. R., and J. C. Swallow (1976), Equatorial undercurrents, *Deep Sea Res. Oceanogr. Abstr.*, *23*, 999–1001.

Macdonald, A. M. (1993), Property fluxes at 30°S and their implications for the Pacific-Indian throughflow and the global heat budget, *J. Geophys. Res.*, *98*, 6851–6868.

Mantyla, A., and J. L. Reid (1983), Abyssal characteristics of the world ocean waters, *Deep Sea Res., Part A*, *30*, 805–833.

Mantyla, A., and J. L. Reid (1995), On the origins of deep and bottom waters of the Indian Ocean, *J. Geophys. Res.*, *100*, 2417–2439.

McCarthy, M. C., and L. D. Talley (1999), Three-dimensional isoneutral potential vorticity structure in the Indian Ocean, *J. Geophys. Res.*, *104*, 13,251–13,267.

McCartney, M. S. (1977), Subantarctic Mode Water, in *A Voyage to Discovery*, edited by M. Angel, pp. 103–119, Elsevier, New York.

McCreary, J. P., P. K. Kundu, and R. L. Molinari (1993), A numerical investigation of dynamics, thermodynamics and mixed-layer processes in the Indian Ocean, *Prog. Oceanogr.*, *31*, 181–244.

Meyers, G. (1996), Variation of Indonesian Throughflow and the El Niño–Southern Oscillation, *J. Geophys. Res.*, *101*, 12,255–12,263.

Meyers, G., R. J. Bailey, and A. P. Worby (1995), Geostrophic transport of Indonesian Throughflow, *Deep Sea Res., Part I*, *42*, 1163–1174.

Miyama, T., T. Awaji, K. Akitomo, and N. Imasata (1995), Study of seasonal transport variations in the Indonesian seas, *J. Geophys. Res.*, *100*, 20,517–20,541.

Molcard, R., M. Fieux, and A. G. Ilahude (1996), The Indo-Pacific Throughflow in the Timor Passage, *J. Geophys. Res.*, *101*, 12,411–12,420.

Molcard, R., M. Fieux, and F. Syamsudin (2001), The throughflow within Ombai Strait, *Deep Sea Res., Part I*, *48*, 1237–1253.

Murray, S. P., and D. Arief (1990), Characteristics of circulation in an Indonesian archipelago strait from hydrography, current measurements and modeling results, in *The Physical Oceanography of Sea Straits*, edited by L. J. Pratt, pp. 3–23, Springer, New York.

Nakano, H., and N. Suginohara (2002), A series of middepth zonal flows in the Pacific driven by winds, *J. Phys. Oceanogr.*, *32*, 161–176.

Postma, H., and W. G. Mook (1988), The transport of water through the east Indonesian deep-sea basins. A comparison of Snellius I and II results, *Neth. J. Sea Res.*, *22*, 378–381.

Quadfasel, D., A. Frische, and G. Cresswell (1996), The circulation in the source area of the South Equatorial Current in the eastern Indian Ocean, *J. Geophys. Res.*, *101*, 12,483–12,488.

Reid, J. L. (1994), On the total geostrophic circulation of the North Atlantic Ocean: Flow patterns, tracers and transports, *Prog. Oceanogr.*, *33*, 1–92.

Reid, J. L. (1997), On the total geostrophic circulation of the Pacific Ocean: Flow patterns, tracers, and transports, *Prog. Oceanogr.*, *39*, 263–352.

Reid, J. L. (2003), On the total geostrophic circulation of the Indian Ocean: Flow patterns, tracers, and transports, *Prog. Oceanogr.*, *56*, 137–186.

Robbins, P. E., and J. M. Toole (1997), The dissolved silica budget as a constraint on the meridional overturning circulation of the Indian Ocean, *Deep Sea Res., Part I*, *44*, 879–906.

Rochford, D. J. (1961), Hydrology of the Indian Ocean. 1. The water masses in intermediate depths of the southeast Indian Ocean, *Aust. J. Mar. Freshwater Res.*, *12*, 129–149.

Rochford, D. J. (1966), Distribution of Banda intermediate water in the Indian ocean, *Aust. J. Mar. Freshwater Res.*, *17*, 61–76.

Roemmich, D. (1983), Optimal estimation of hydrographic station data and derived fields, *J. Phys. Oceanogr.*, *13*, 1544–1549.

Schmitz, W. J. (1995), On the interbasin-scale thermohaline circulation, *Rev. Geophys.*, *33*, 151–174.

Schott, F., and J. P. McCreary (2001), The monsoon circulation of the Indian Ocean, *Prog. Oceanogr.*, *51*, 1–123.

Shetye, S. R., S. S. C. Shenoi, A. D. Gouveia, G. S. Michael, D. Sundar, and G. Nampoothiri (1991), Wind-driven coastal upwelling along the western boundary of the Bay of Bengal during the southwest monsoon, *Cont. Shelf Res.*, *11*, 1397–1408.

Smith, W. H. F., and D. T. Sandwell (1997), Global seafloor topography from satellite altimetry and ship depth soundings, *Science*, *277*, 1957–1962.

Smith, W. H. F., and P. Wessel (1990), Gridding with continuous curvature splines in tension, *Geophysics*, *55*, 293–305.

Sonnerup, R. E., P. D. Quay, and J. L. Bullister (1999), Thermocline ventilation and oxygen utilization rates in the subtropical north Pacific based on CFC and 14C distributions during WOCE, *Deep Sea Res., Part I*, *46*, 777–805.

Speich, S., B. Blanke, and G. Madec (2001), Warm and cold water routes of a GCM thermohaline conveyor belt, *Geophys. Res. Lett.*, *28*, 311–314.

Sprintall, J., S. Wijffels, T. Chereskin, and N. Bray (2002), The JADE and WOCE I10/IR6 throughflow sections in the southeast Indian Ocean. Part 2: Velocity and transports, *Deep Sea Res., Part II*, *49*, 1363–1390.

Sprintall, J., S. Wijffels, A. L. Gordon, A. Ffield, R. Molcard, R. D. Susanto, I. Soesilo, J. Sopaheluwakan, Y. Surachman, and H. M. van Aken (2004), A new international array to measure the Indonesian Throughflow: INSTANT, *Eos Trans. AGU*, *85*, 372–376.

Talley, L. D. (1996), Antarctic Intermediate Water in the South Atlantic, in *The South Atlantic: Present and Past Circulation*, edited by G. Wefer et al., pp. 219–238, Springer, New York.

Talley, L. D. (2003), Shallow, intermediate and deep overturning components of the global heat budget, *J. Phys. Oceanogr.*, *33*, 530–560.

Talley, L. D., and M. O. Baringer (1997), Preliminary results from WOCE hydrographic sections at 80E and 32S in the central Indian Ocean, *Geophys. Res. Lett.*, *24*, 2789–2792.

Talley, L. D., and G. C. Johnson (1994), Deep, zonal subequatorial flows, *Science*, *263*, 1125–1128.

Top, Z., A. Gordon, P. Jean-Baptiste, M. Fieux, I. G. Ilahude, and M. Muchtar (1997), He in Indonesian seas: Inferences on deep pathways, *Geophys. Res. Lett.*, *24*, 547–550.

Van Aken, H. M., J. Punjana, and S. Saimima (1988), Physical aspects of the flushing of the east Indonesian basins, *Neth. J. Sea Res.*, *22*, 315–339.

Van Aken, H. M., A. J. Van Bennekom, W. G. Mook, and H. Postma (1991), Application of Munk abyssal recipes to tracer distributions in the deep waters of the South-Banda Basin, *Oceanol. Acta*, *14*, 151–162.

Van Bennekom, A. J. (1988), Deep water transit times in the eastern Indonesian basins calculated from dissolved silica in deep and interstitial waters, *Neth. J. Sea Res.*, *22*, 341–354.

Van Bennekom, A. J., and M. Muchtar (1988), Reactive phosphate in the eastern Indonesian seas, *Neth. J. Sea Res.*, *22*, 361–367.

Van Bennekom, A. J., W. W. Kastoro, and W. C. Patzert (1988), Recirculation in the Banda Throughflow, traced with dissolved silica, *Neth. J. Sea Res.*, *22*, 355–359.

Van Riehl, P. M. (1943), Introductory remarks and oxygen content, in *The Snellius Expedition*, vol. II, *Oceanographic Remarks,* part V, *The Bottom Water,* 77 pp., E. J. Brill, Cologne, Germany.

Vranes, K., A. L. Gordon, and A. Ffield (2002), The heat transport of the Indonesian Throughflow and implications for the Indian Ocean heat budget, *Deep Sea Res., Part II*, *49*, 1391–1410.

Warren, B. A. (1981), Transindian hydrographic section at lat. 18°S: Property distributions and circulation in the south Indian Ocean, *Deep Sea Res., Part A*, *28*, 759–788.

Waworuntu, J. M., R. A. Fine, D. B. Olson, and A. L. Gordon (2000), Recipe for Banda Sea water, *J. Mar. Res.*, *58*, 547–569.

Wessel, P., and W. H. F. Smith (1998), New, improved version of Generic Mapping Tools released, *Eos Trans. AGU*, *79*, 579.

Wijffels, S. (2001), Ocean transport of fresh water, in *Ocean Circulation and Climate*, edited by G. Siedler, J. Church, and J. Gould, pp. 475–488, Elsevier, New York.

Wijffels, S., J. Sprintall, M. Fieux, and N. Bray (2002), The JADE and WOCE I10/IR6 throughflow sections in the southeast Indian Ocean. Part 1: Water mass distribution and variability, *Deep Sea Res., Part II*, *49*, 1341–1362.

Wyrtki, K. (1961), Physical oceanography of the Southeast Asian waters, *NAGA Rep. 2*, 195 pp., Scripps Inst. of Oceanogr., La Jolla, Calif.

Wyrtki, K. (1973), An equatorial jet in the Indian Ocean, *Science*, *191*, 262–264.

You, Y. (1998a), Dianeutral mixing and transformation of Antarctic Intermediate Water in the Indian Ocean, *J. Geophys. Res.*, *103*, 30,941–30,971.

You, Y. (1998b), Intermediate water circulation and ventilation of the Indian Ocean derived from water-mass contributions, *J. Mar. Res.*, *56*, 1029–1067.

You, Y., and M. Tomczak (1993), Thermocline circulation and ventilation in the Indian Ocean derived from water mass analysis, *Deep Sea Res., Part I*, *40*, 13–56.

Young, W. R., and P. B. Rhines (1982), A theory of the wind-driven circulation II. Gyres with western boundary layers, *J. Mar. Res.*, *40*, 849–872.

Zhang, H.-M., and L.D. Talley (1998), Heat and buoyancy budgets and mixing rates in the upper thermocline, *J. Phys. Oceanogr.*, *28*, 1961–1978.

J. Sprintall and L. D. Talley, Scripps Institution of Oceanography, University of California, San Diego, La Jolla, CA 92093-0230, USA. (jsprintall@ucsd.edu; ltalley@ucsd.edu)